Geochemistry 84 (2024) 126204

Contents lists available at ScienceDirect

Geochemistry

journal homepage: www.elsevier.com/locate/chemer

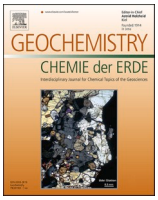

Alunite and kaolinite as geochemical markers in active acid sulfate alterations of southern Italy (Panarea, La Solfatara and Ischia)

Théo Bouvart [a,*], Julien Poot [a], Augustin Dekoninck [b], Flore Schmit [a], Maxime Keutgen De Greef [c], Jacqueline Vander Auwera [d], Alain Bernard [b], Johan Yans [a]

[a] Institute of Life-Earth-Environment (ILEE), University of Namur, 61 rue de Bruxelles, B-5000 Namur, Belgium
[b] Laboratoire G-Time, Department of Geosciences, Environment and Society (DGES), Université Libre de Bruxelles (ULB), 50, Av. FD Roosevelt, Brussels 1050, Belgium
[c] Atmospheric and Oceanic Sciences Program, Princeton University, 300 Forrestal Road, Sayre Hall Princeton, NJ 08540-6654, United States of America
[d] Département de Géologie, Université de Liège, 4000 Sart Tilman, Belgium

ARTICLE INFO

Handling Editor: Kailasa Pandarinath

Keywords:
Hydrothermal
Alteration
Geochemistry
Indices
Acid-sulfate
Italy
Alunite
Kaolinite

ABSTRACT

Hydrothermal alteration is a common process in volcanic and geothermally active areas. Interactions between host rock and hot, often acidic, fluids induce significant changes in texture, mineralogy, and geochemistry of the protolith, potentially impacting volcanoes stability. Southern Italy's volcanic regions are geothermally active, exhibiting conspicuous hydrothermal activity. Here, we focus on active hydrothermal acid-sulfate alteration in calc-alkaline (Panarea) and alkaline (Ischia - Solfatara) volcanic products in order to (1) spatially identify alteration assemblages using XRD, (2) determine the mobility of major and trace elements during hydrothermal alteration processes using FUS and ICP-MS, (3) estimate and compare the degree of alteration using alteration indices and elemental ratios. Our data reveal sulfur and sulfates sublimate next to the fumarole fields. Nearby fumaroles, alunite and kaolinite are the most abundant mineral phases in the alteration assemblages, often associated with amorphous silica, iron(hydr)oxides, smectites and gypsum. Kaolinite is rarely observed in La Solfatara assemblage. Comparison between the protolith and the alteration products geochemistry indicates that alteration retains the calco-alkaline or alkaline heritage, which confirms the usefulness of some chemical indices (PIA vs AI; (La + Ce)/Y vs (Zr + Hf)/(Ta + Nb) for alteration products. Despite comparable mineralogies, various degrees of alteration are observed in La Solfatara, Panarea and Ischia, constraining the alunite or kaolinite formation and highlighting local vs. global geochemical behaviors. We conclude that the (im)mobility of chemicals elements within the hydrothermal alteration - such as HFSE, REE or alkali - is mainly controlled by the protolith composition, the alteration intensity and mineralogy, pH, ionic strength and possibly crystallinity of alteration minerals.

1. Introduction

Hydrothermal alteration is a common process in volcanic and geothermally active areas, which activity is manifested by fumarolic fields and/or acid crater lakes at the surface (Boyce et al., 2007; Mayer et al., 2016). In the upper part of the hydrothermal system, water interacts with degassing magmatic bodies creating hot and often acidic fluids at or above the water table/sea level by oxidation of H_2S (Rye, 2005; Mayer et al., 2016). The fresh volcanic rocks (also called protoliths) interact with acid solutions inducing changes in texture, mineralogy and geochemistry. Fluid circulation within drains enables interaction with the protoliths. Cooling and progressive neutralization of fluids leads to new paragenesis (Boyce et al., 2007). Hydrothermal alteration can also modify some intrinsic physical and mechanical properties of the protolith such as porosity, permeability and density that can jeopardize the volcano stability (Heap et al., 2021). Comparison of this phenomenon among different systems helps to understand the mechanisms of hydrothermal alteration and the impact of protolith and fluid compositions on the resulting mineralogy and geochemistry. The main factors controlling alteration are the composition of the protolith and the fluids as well as pH, temperature, pressure and duration of the interaction between hydrothermal fluid and rock.

The convergence between the Eurasian and African tectonic plates produced volcanism due to subduction and extension in the southern

* Corresponding author at: University of Namur, 61 rue de Bruxelles, B-5000 Namur, Belgium.
E-mail address: theo.bouvart@unamur.be (T. Bouvart).

https://doi.org/10.1016/j.chemer.2024.126204
Received 16 May 2024; Received in revised form 8 October 2024; Accepted 13 October 2024
Available online 24 October 2024

part of the Tyrrhenian Sea since the Miocene. Plio-Quaternary volcanism in the circum-Tyrrhenian area exhibits variable rock compositions from calc-alkaline to alkaline volcanic rocks (Peccerillo and Lustrino, 2005). Some volcanic regions of Southern Italy are also geothermally active and hydrothermal alteration is conspicuous. The intensity of hydrothermal alteration changes over time, as indicated by fluid analysis (Chiodini et al., 2011) and changes in neoformed minerals in the same area (Piochi et al., 2019). Continuous geophysical and thermal monitoring of these hydrothermal systems also show variations in hydrothermal fluxes (Di Giuseppe et al., 2015).

This study focuses on active hydrothermal acid-sulfate alteration of varying intensities on calc-alkaline (Panarea) and alkaline (Ischia - Solfatara) volcanic products in the circum-Tyrrhenian area. These steam heated environments have led to advanced argillic alteration (Chiodini et al., 2006; Piochi et al., 2015, 2019), characterized by specific fractionation of major and trace elements, including rare earth elements (REE), in alteration products found in and nearby the fumarole areas. In each sampling site, the alteration zones as well as the geochemistry of their mineralogical assemblages are identified. We provide an interpretation based on alteration indices (Pandarinath, 2022) and we discuss the global and specific geochemical behaviors of acid-sulfate alteration products arising in these different hydrothermal systems.

2. Geological settings

2.1. Aeolian Islands: Panarea

Panarea is the result of a large partially emerged lava dome strato-volcano. This caldera is located in the eastern Aeolian Islands (Fig. 1a) (Calanchi et al., 2002). The main volcanic products belong to epochs 1

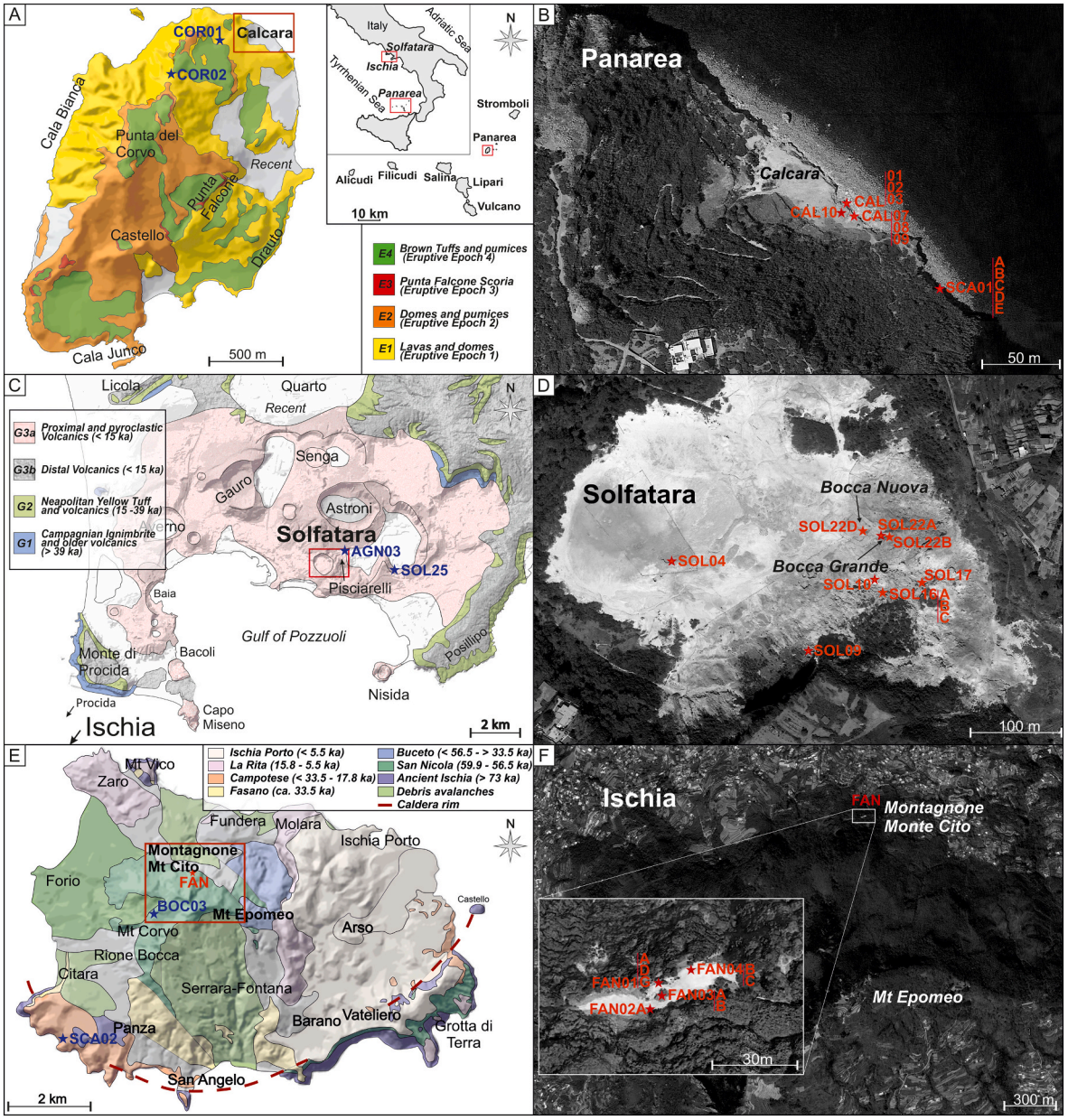

Fig. 1. Location of sampling sites: blue stars are fresh rocks (=protolith), and red stars are altered rocks. (A) Simplified geological map of Panarea modified from (Lucchi et al., 2013). (B) Google Earth view of Calcara and surroundings. (C) Simplified geological map of Phlegrean Fields caldera modified from (Mayer et al., 2016). (D) Google Earth view of La Solfatara crater. (E) Simplified geological map of Ischia modified from (Piochi et al., 2019) and (F) Google Earth view of the Mt. Epomeo - Montagnone - Mt. Cito area and close up on the sampling area. (For interpretation of the references to color in this figure legend, the reader is referred to the web version of this article.)

(155–127 ka) and 2 (127–118 ka) during which massive lava domes were formed. During eruptive epochs 3 (100 ka) and 4 (54–8.7 ka), volcanic products were scoria, pumice and tuff deposits. The latter come from islets being part of the Panarea volcanic complex, revealing explosive episodes (Calanchi et al., 2002; Lucchi et al., 2013). Rocks range from calc-alkaline to high-K calc-alkaline (CA-HKCA) basaltic andesite to rhyolite. A large area is still affected by mainly submarine fumarolic activity (Italiano and Nuccio, 1991; Chiodini et al., 2006; Capaccioni et al., 2007; Tassi et al., 2009). Chemical variations and $^3He/^4He$ isotopes suggest a magmatic system at relatively shallow depth, centered on or close to Bottaro fumaroles (part of the Panarea volcanic complex caldera- submarine vents (Fig. 1a) (Capaccioni et al., 2007). Both Bottaro and La Calcara (main island) show synchronous variations suggesting the same deep feeding magmatic gas system and similar processes responsible for chemical variations (Italiano and Nuccio, 1991; Capaccioni et al., 2007). Fluids typically originate from seawater, which is chemically modified by complex interactions with boiling volcanic gases and, on the mainland, meteoric water (Tassi et al., 2009).

2.2. Gulf of Naples: Solfatara and Ischia

The Campanian Volcanic Province comprises active volcanoes such as Somma-Vesuvio, Phlegrean Fields, Ischia, Procida, but also the islands of Ponza, Palmarola, Santo Stefano and Ventotene (Colella et al., 2017). The Phlegrean Fields area lies in the Campanian Plain graben delimited to the west by the Tyrrhenian Sea basin and to the east, north and south by the Apennine belt (Piochi et al., 2014). The graben results from Pliocene and Quaternary extensional tectonics that opened the southern Tyrrhenian Sea basin. A wide system of regional NW–SE and NE–SW transfer faults trending connects the Tyrrhenian bathyal plain to the continental area (Orsi et al., 1996; Piochi et al., 2014).

The structural depression of the Phlegrean Fields is widely interpreted as a long-lived caldera system formed over the last 50,000 years (Fig. 1c). Two major eruptions took place: the Campanian Ignimbrite (CI: 39,000 years) and the Neapolitan Yellow Tuff (NYT: 12,000 years) (Di Vito et al., 1999). Both were supplied by trachyte and phonolite magmas (Tomlinson et al., 2012). CI consists of alkali-rich trachytic tuff. NYT is characterized by its great heterogeneity (Scarpati et al., 1993). Pyroclastic-flow and minor fall deposits have two different facies: lithified and non-lithified. The lithification is the result of a diagenetic zeolithisation process (Scarpati et al., 1993). The Phlegrean Fields caldera is the most active and largest feature of the Phlegrean Volcanic District. The last eruption occurred in 1538 CE (Monte Nuevo), bradyseism and fumarolic activity testified that the system is still active (Orsi et al., 1996; Chiodini et al., 2011; Mayer et al., 2016). The two main fumaroles of the Solfatara are Bocca Grande (BG) and Bocca Nuova (BN) (Caliro et al., 2007) – Fig. 1d. They have similar chemical compositions and consist of water, CO_2, H_2S, N_2, H_2, CH_4, He and CO (Chiodini et al., 2015).

CO_2/CH_4 and He/CH_4 ratios in the fumarolic fluids suggest that magmatic gas pulses are being injected into the hydrothermal system through a high-permeability zone located approximately 2 km beneath the surface (Chiodini et al., 2022). This injection process changes in frequency and intensity and triggers the short-term uplifting episode observed over the past 40 years. It also contributes to seismic activity as some hypocenters of the recent earthquakes are consistent with the fluid injection zone depths (Chiodini et al., 2021). During peaks of hydrothermal activities (1985, 1990 and 1995) the gas had a higher magmatic fraction, up to 50 % (Caliro et al., 2007). An increase of the magmatic flux is also responsible for heating the system, causing ground inflation observed since 2005 (Chiodini et al., 2015). CO_2/H_2O ratio shows an increasing trend since the early 2000's which indicates CO_2 addition from a magmatic source, partial steam condensation and possibly the decarbonation of hydrothermal calcite favored by heating the hydrothermal reservoir (Orsi et al., 2021).

Ischia Island is in the Gulf of Naples ~8 km west from the coast (Fig. 1e) and is considered as a rare case of well-exposed, young and continuous caldera resurgence, associated with uplifts of the intracaldera rocks (Acocella and Funiciello, 1999). Volcanism at Ischia is connected to the activity of Phlegrean Fields (Crisci et al., 1989). Volcanic activity started at least 150,000 years ago and can be divided into three volcanic cycles: (1) The first one (55,000–33,000 years BP) started with the caldera-forming Monte Epomeo Green Tuff eruption (Brown et al., 2014). Several collapses occurred during this period generating a 10 × 7 km-diameter caldera. (2) The second cycle (28,000–18,000 years BP) started with magmatic activities that progressively mixed with the residual and differentiated magma of the first cycle (Brown et al., 2014). This new supply of shoshonitic magma probably triggered the resurgence of the caldera and fed the eruption of the Grotta di Tera 5 about 28,000 years ago (Orsi et al., 1999). (3) The last cycle (10,000 BP – 1302 CE) was characterized by latitic to phonolitic magmas eruptions (Brown et al., 2014), and the last erupted deposits (Arso lavas and pyroclastics) date back to 1301–1302 CE (Sbrana et al., 2018).

Otherwise, the Ischia hydrothermal system consists of different contributions from meteoric water, sea water and thermal fluids rising from possibly two distinct hydrothermal reservoirs. In the southwestern part of the island, (Di Napoli et al., 2009) proposed that those two reservoirs overlap and are ~200 and ~ 1000 m deep with temperatures of ~150 °C and ~ 270 °C, respectively (Carlino et al., 2014). CO_2, H_2S, H_2, CO, CH_4 and $^3He/^4He$ ratios indicate a supply by a deep-rising gas component, likely of magmatic origin, in those reservoirs (Di Napoli et al., 2009). Ischia Island sends out manifold fumaroles and hot springs with maximum surface temperature of about ~100 °C (Carlino et al., 2014).

3. Materials and methods

Protoliths and alteration products were collected between July and September 2016 on Panarea, Solfatara and Ischia. Protolith samples were collected as fresh as possible outside the alteration zones (Fig. 1a, c, e). Alteration products were collected based on their macro-mineralogy and textures. Fracture fillings in lavas and replacement deposits in tuffs as well as mudpools were also sampled. 36 were selected for geochemical analyses. These 36 samples were selected in alteration zones, from the center of the acid and hot emanations to their periphery, to observe the mineralogy and associated geochemical evolutionary patterns.

XRD was conducted on the 36 samples selected for geochemistry. Samples were crushed using a RETSCH PM 100 planetary ball mills (UNamur). XRD analyses on powdered samples were performed using X-Ray Panalytical X'Pert Pro diffractometer and a PHILLIPS PW3710 (CuKα radiation), at the PC2 platform (UNamur), operating at 40 kV and 30 mA.

In addition, five (5) clay fractions (< 2 μm) were prepared to identify specific clay minerals: samples were mixed with distilled water after grinding, and the solutions were then decanted for 24 h to separate coarse and fine mineral fractions. Samples were washed in hot water (~80 °C) to dissolve gypsum and salt to avoid peak overlapping. The samples were sedimented and the <2 μm fraction was collected. The <2 μm fraction was then saturated with calcium via a 1 M $CaCl_2$ solution. Samples were centrifuged and rinsed several times. Oriented aggregates were then deposited on glass slides. Oriented aggregates were further treated with ethylene glycol and heated at 550 °C.

Thin sections were studied on 7 fresh volcanic rocks and 8 mid-alteration products containing residual altered primary mineral phases and textures.

Whole rock geochemistry was carried out on the 36 crushed samples (maximum 125 μm granulometry) with respect to the different mineralogical assemblages previously identified by XRD. Major elements were quantified by FUS-ICP (Fusion Inductively Coupled Plasma Optical Emission Spectrometry) while traces elements, including rare earth

elements (REE), were quantified by FUS-MS (Fusion Mass Spectrocopy). Reduced Iron (FeO) was determined by titration (detection limit 0.1 %), as well as sulfur (S) (detection limit 0.01 %) and sulfate (SO_4) (detection limit 0.05 %) at Activation Laboratories Ltd. (Canada). All whole-rock analyses and detection limits are given in Supplementary Data.

4. Results

4.1. Mineralogy & associated textures

4.1.1. Protoliths

4.1.1.1. Panarea. Protoliths collected in Panarea range from basalts to dacites (Fig. 2a). Textures are mainly porphyritic to amygdaloid with phenocrysts of zoned plagioclase (An_{10} to An_{50}), clinopyroxene and orthopyroxene, amphibole, sanidine and rare olivine within a glassy mesostasis. Many xenoliths are found inside the lava flows (Fig. 3a), as also observed by Calanchi et al., 2002; Doherty et al., 2015; Lucchi et al., 2013. Zoned and twinned plagioclase represent >50 % of the phenocrysts with size reaching 500 μm to 3 mm. Other phenocrysts, such as pyroxenes and less frequently hornblende, can be inserted between the twinned plagioclase displaying intergranular to glomeroporphyric textures. Glassy inclusions give a dusty texture to most plagioclase crystals as well. The composition of the clinopyroxene is diopside - augite while orthopyroxene is mainly hypersthene. Little composition variability is observed. COR1 and COR2 from eruptive epoch Ic (132–127 ka) were selected as protoliths.

4.1.1.2. Solfatara. The volcanic products sampled in Solfatara are crumbly pumices and lapillis rich trachytic tuffs belonging to the NYT (Fig. 2a). Thin sections reveal that the samples are vesicular porphyric trachyte containing volcanic glass, sanidine (up to 50 %), Ca-plagioclase, augite, hornblende, biotite and muscovite phenocrysts. Some smectite are also found as part of the late mineralogy. AGN3 sample shows some late zeolites such as chabazite, analcime and phillipsite. Alkali-trachytic glass is the main phase of the samples. AGN3 and SOL25 from eruptive epoch III (5.5–3.8 ka) are the freshest samples and were chosen as protolith references for comparison with altered products.

4.1.1.3. Ischia. Protoliths are tuffs and pumices of trachytic to phonolitic composition as well as trachytic lavas (Fig. 2a). Vesicular and porphyric tuffs are rich in lapillis and pumices. The total phenocrysts content reaches 30 % and is exceptionally as high as 40 %. Sanidine is the dominant mineral with a long axis up to 3 mm, followed by biotite. Additional phenocrysts are muscovite and clinopyroxene. The microlithic matrix is made of the same mineral assemblage. Lavas show some phenocrysts of hornblende and ilmenite. Clinopyroxene crystals are zoned and rare, mostly as microphenocrysts. BOC3 from eruptive epoch II (59.9–56.5 ka) and SCA2 from eruptive epoch IV (33–13 ka) are selected as representing the unaltered protoliths.

4.1.2. Altered samples - secondary mineralogy

4.1.2.1. Panarea. Stockwork mineralization occurs along hydrothermal veins, vents and breccias, revealing the upper roots of the hydrothermal system (Fig. 3e, f). Sulfides are found north of La Calcara and composed of pyrite, silica, alunite and native sulfur. Those assemblages take only place in veins close to active hydrothermal fields of La Calcara and sea level. Nearby this assemblage, baryte, hematite, goethite, alunite and gypsum are also identified. Kaolinite and halite are accessory phases.

Three assemblages have been analyzed. Samples CAL1–3 and samples CAL7–10 respectively belong to the first and second assemblages (Fig. 3c, d). Assemblages is, from inside outward, amorphous silica, native sulfur, alunite, kaolinite, gypsum (Fig. 3c, d). Samples CAL7 and 8 have significant kaolinite/alunite interstratification and iron oxides (Table 1). Sample CAL9 is almost pure kaolinite. These samples were collected from inside outward of the alteration vents (Fig. 3d). Close to active hydrothermal vents of La Calcara, textures are porous and clayey (Fig. 3d). Alunite is widely common alongside kaolinite and may be present in greater quantities in the vicinity of active fumaroles, in association or not with kaolinite. Kaolinite is mainly found a few meters from active fumaroles. Pervasive subvertical structures are observed on top of the fumaroles patches. Intruding veins and veinlets are typically white and straight cutting blocks and boulders that have ghost textures (Fig. 3e). Fractures, veins and veinlets are filled with gypsum, alunite, and kaolinite.

The third mineral assemblage is observed in samples SCA1A-E which were taken from outside inward of the spherical breccia zone. Rounded breccias were formed in the interstices of the decompression of the andesitic prisms (samples series SCA1 - Fig. 3b). Besides, their mineralogy evolves from outside to inside: kaolinite (± alunite), hematite, smectite associated with altered primary phases of the protolith like residual cristobalite, plagioclase, pyroxenes and amphiboles (Table 1). The center of the breccia presents ghost textures, mainly plagioclase, due to the dissolution of the minerals (Fig. 3b). The XRD data suggest that the content and crystallinity of kaolinite tends to increase inward.

4.1.2.2. Solfatara. The first assemblage, collected a few meters from the active vents, is alunite rich (SOL16A, B, C and SOL17), which is the major phase in the Solfatara (Fig. 4c, d). The second assemblage, collected around of the fumarole areas with a typical "solfataratic" looking contains mostly alunite associated with native sulfur (SOL10), gypsum or alunogen ($Al_2(SO_4)_3{\cdot}17H_2O$) as well as some residual cristobalite (SOL4,9 - Table 1). The XRD data indicate that sublimate samples from the third assemblage SOL22B from the Bocca Grande fumarole zone contains alunogen, salammoniac (NH_4Cl), mascagnite ($(NH_4)_2SO_4$) and russoite ($NH_4ClAs_2O_3(H_2O)_{0.5}$) while sample SOL22D contains amorphous silica, sanidine and even calcite (Fig. 4e - Table 1). Within the most active hydrothermal vents, native sulfur generally occurs as acicular crystals and as impregnation and idiomorphic crystals. The mineralization also includes amorphous silica, rutile, calcite and illite. Amorphous silica is arranged as pseudomorphs after protolith minerals such as amphibole, pyroxenes and feldspar (mostly sanidine).

4.1.2.3. Ischia. Two assemblages have been analyzed. From the center to the outside of the fumarole, the first assemblage is composed of FAN1A, FAN1D and FAN1G. XRD shows that FAN1A is composed of halotrichite ($FeAl_2(SO_4)_4{\cdot}22H_2O$), pickeringite ($MgAl_2(SO_4)_4{\cdot}22H2O$), alum-(K) ($KAl(SO_4)_2{\cdot}12(H_2O)$), apjohnite ($MnAl_2(SO_4)_4{\cdot}22H_2O$) and quartz (Table 1). Sulfates form flange-shaped tiny efflorescence (Fig. 5f) close to dendritic aggregates of native sulfur. Needle-like halotrichite is associated with alunogen and grows on the alunogen crystals. Amorphous silica is also identified close to the vents. The second assemblage collected nearby the fumarole FAN2B, FAN3A&B, FAN4C&D is homogeneous (Table 1). Alunite and kaolinite are the two most abundant phases in the altered samples (FAN1A, B, G &, FAN3A&B, FAN4B&C) from Ischia (Fig. 1e, f). Kaolinite and alunite are often interbedded. Gypsum is associated with clay minerals and occasionally with other sulfates. Alum-(K) and alunite crystals may show similar habits and sizes. Reddish color of the rocks is given by hematite (Fig. 5d). Clay-rich samples (kaolinite and smectite) are generally observed with primary minerals such as feldspar (sanidine), chabazite-K and biotite.

4.2. Geochemistry

4.2.1. Protoliths

In Panarea, Fe_2O_{3t}, MgO, Al_2O_3, CaO decrease whereas Na_2O and K_2O increase with increasing SiO_2 content from basaltic andesites to dacites (Fig. 2a, b). In Solfatara, the alkaline trend ($Na_2O + K_2O$ up to 12

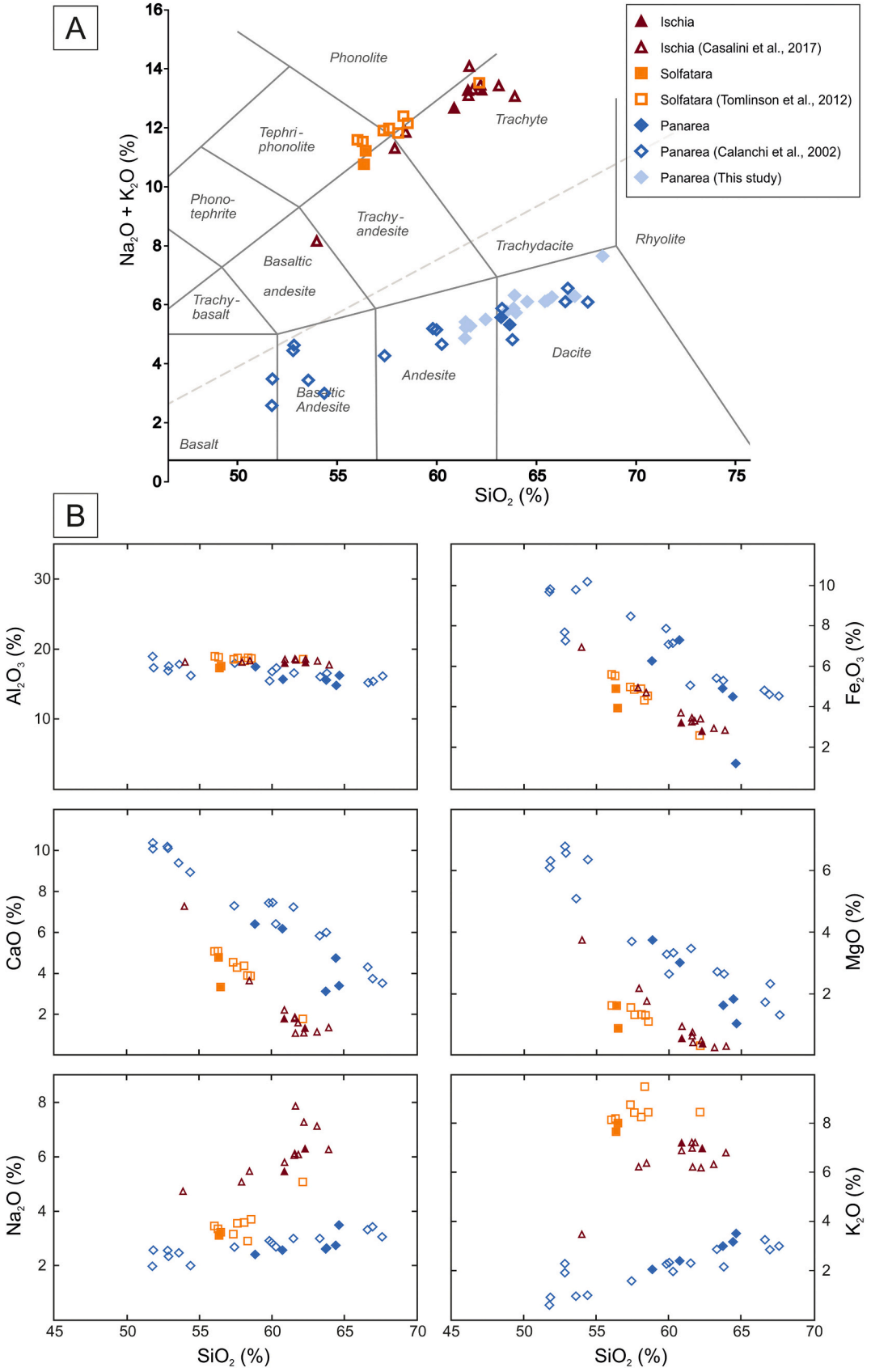

Fig. 2. (A) Total alkali vs. silica (TAS) diagram from (Le Bas et al., 1986) and (B) major elements variation diagrams of some volcanic products from La Solfatara (Tomlinson et al., 2012), Ischia (Casalini et al., 2017) and Panarea (Calanchi et al., 2002), including samples from this study (filled symbols).

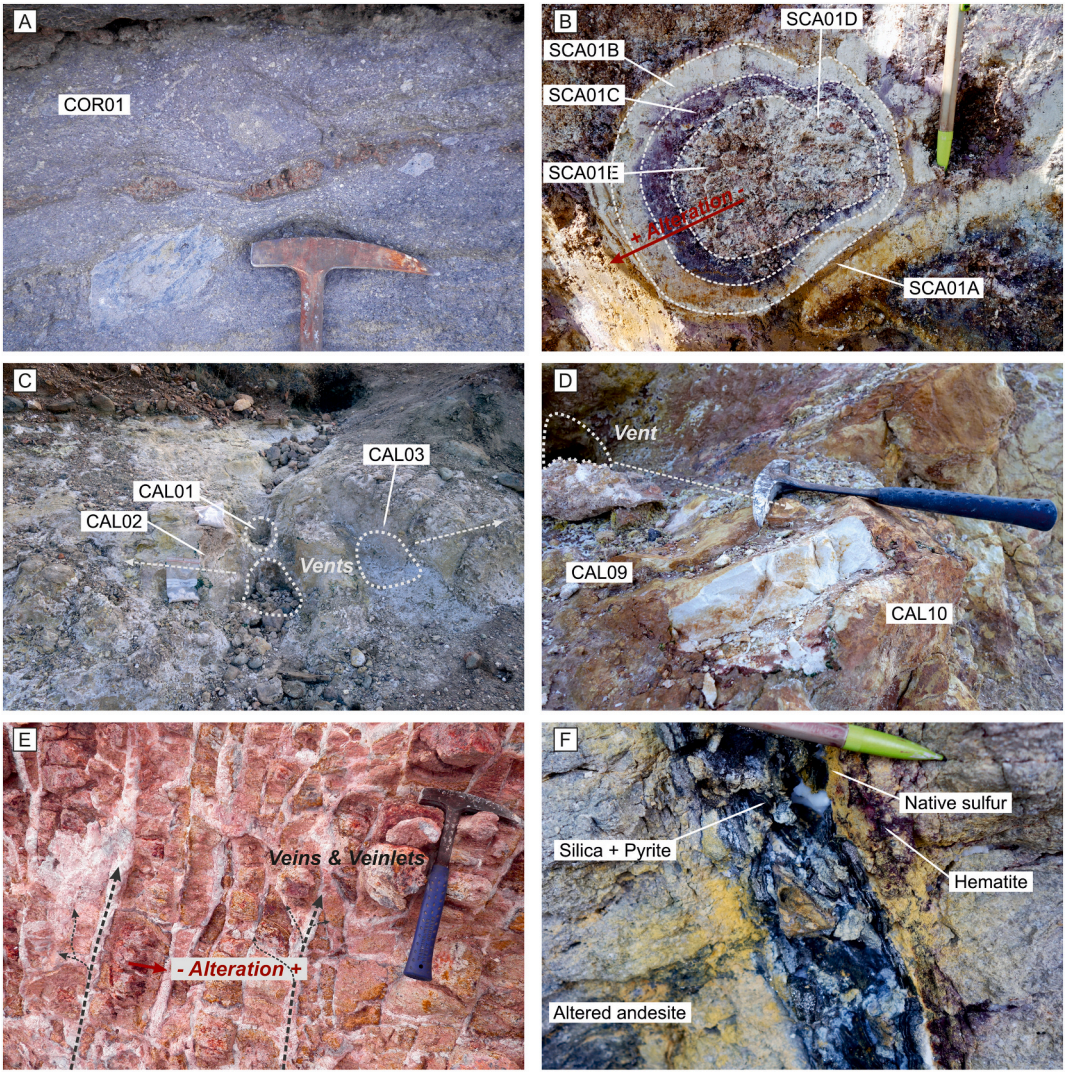

Fig. 3. Field pictures of representative samples collected on Panarea. (A) Andesite (protolith COR01) with massive xenoliths in the flow. (B) Altered andesitic column with alteration gradient (SCA assemblage). (C) Samples collected in the fumaroles area of La Calcara. (D) Massive kaolinite deposits in Spaggia della Calcara. (E) Veins and veinlets cutting through andesite on top of hydrothermal system. (F) Onshore sulfide veins deposits at La Calcara North.

%) of the trachytic tuffs display decreasing Fe_2O_{3t}, MgO, Al_2O_3, CaO and increasing Na_2O and K_2O with increasing SiO_2 (Fig. 2a, b). However, SOL25 and AGN3 have a similar composition. In Ischia, trachyte and trachyandesite from Ischia exhibit a high total alkali ($Na_2O + K_2O$ up to 13 %, Fig. 2a). Trends from biplot diagrams show inverse correlation in Fe_2O_{3t}, MgO, Al_2O_3 and CaO and direct correlation in Na_2O and K_2O with respect to SiO_2 content (Fig. 2a, b).

4.2.2. *Altered samples compared to protolith composition*

4.2.2.1. Mass change. Binary Al_2O_3/Hf and Zr/Al_2O_3 correlation was used to estimate the mobility of elements and the correlation coefficient between protolith and alteration products (Fig. 6) as similar concentrations in protoliths and altered rocks suggesting immobility of these elements. Although some of the Al_2O_3/Hf and Zr/Al_2O_3 ratios from alteration products are close to the protolith, a large proportion of the samples are distributed along a linear trend away from the protolith cluster, showing a strong correlation coefficient (Fig. 6). These opposite distribution trends reflect the changes in Al mass during the alteration process at each site. A reconstructed composition of the samples is therefore approximated by the equation (MacLean, 1990):

$$RC = \frac{IM_p}{IM_a} * C_a \quad (1)$$

The formula for computing the reconstructed composition of an element (RC) involves the concentrations of immobile element in the altered products (IM_a) and in the average protolith (IM_p) as a ratio and the computed element. Here, we consider an average Hf composition of the local protoliths to mitigate magmatic differentiation and other small primary variations between protoliths from the same study site. This approach presents a degree of approximation, estimated at ±10 % at Ischia and La Solfatara and ± 12 % at Panarea, but makes the protolith homogeneous and unique. Using Eq. (1), variations in the chemical composition of hydrothermally altered products are displayed with respect to their protolith. Then, loss or gain in all elements are computed to monitor the mobility of the elements during hydrothermal alteration which will be discussed in the later sections.

4.2.2.2. Panarea. The first (CAL2, 1, 3) and second assemblages (CAL10, 9, 8, 7) of La Calcara are from an active fumarole zone (Fig. 3c, d). The first assemblage (CAL1–3) is depleted in Cs, Rb and K (Fig. 7a). Enrichment Pb in the CAL1 sample is up to 8 times the average protolith composition (Fig. 7a) while Ba and Sr are slightly enriched and Cs, Rb,

Table 1
Samples location (see Fig. 1 A-F), type and mineralogy. Pg – Plagioclase, Snd – Sanidine, Px – Pyroxene, Musc – Muscovite, Hb- Hornblende, Qz – Quartz, Or – Orthose, Ilm – Ilmenite, Sal – Salammoniac, Rus – Russoite, Masc – Mascagnite, S- Native sulfur, Hal – Halotrichite, Pick – Pickeringite, Alum – Almum-K, Apj – Ajohnite, Am. Si – Amorphous silica, Al – Alunite, Kao – Kaolinite, Gyp – Gypsum, Sm – Smecite, Ba – Baryte, Fe-ox – Iron oxydes, An – Anatase, Ca – Calcite, (r) – residual.

	Sample	Location	Type	Mineral assemblage
Panarea	COR1	N38°38′42.4″ E15°4′13.4”	Protolith - Dacite	Pg, Px, Hb, Or
	COR2	N38°38′37.6″ E15°4′4.4”	Protolith - Dacite	Pg, Px, Hb, Or
	SCA1A	N38°38′41.5″ E15°4′32.3”	Altered andesite prism	Kao, Fe-ox, Alu
	SCA1B	N38°38′41.5″ E15°4′32.3”	Altered andesite prism	Kao, Alu
	SCA1C	N38°38′41.5″ E15°4′32.3”	Altered andesite prism	Kao
	SCA1D	N38°38′41.5″ E15°4′32.3”	Altered andesite prism	Kao, Alu
	SCA1E	N38°38′41.5″ E15°4′32.3”	Altered andesite prism	Sm, Kao, Fe-ox, Pg (r)
	CAL1	N38°38′43.2″ E15°4′30.3”	Hydrothermally altered materials	Am. Si, Kao, An
	CAL2	N38°38′43.2″ E15°4′30.3”	Hydrothermally altered materials	Alu, Kao, Ba
	CAL3	N38°38′43.2″ E15°4′30.3”	Hydrothermally altered materials	Kao, An
	CAL7	N38°38′43.5″ E15°4′29.8”	Hydrothermally altered materials	Kao, Alu, Fe-ox, Qz
	CAL8	N38°38′43.5″ E15°4′29.8”	Hydrothermally altered materials	Kao, Alu, Fe-ox
	CAL9	N38°38′43.5″ E15°4′29.8”	Hydrothermally altered materials	Kao, Alu, Qz
	CAL10	N38°38′43.5″ E15°4′29.8”	Hydrothermally altered materials	Kao
	AGN3	N40°49′51.3″ E14°8′45.6”	Protolith - Tephiphonolite	Snd, Pg, Px, Musc
	SOL25	N40°49′15.3″ E14°09′27.9”	Protolith - Trachyandesite	Snd, Pg, Px, Phil, Musc
	SOL4	N40°49′37.1 E14°08′21.7”	Mudpool	Alu, Gyp, Alug
	SOL9	N40°49′33.4″ E14°8′27.7”	Hydrothermally altered materials	Alu, Snd (r), Gyp
	SOL10	N40°49′35.8″ E14°08′29.1”	Hydrothermally altered materials	Alu, S, Snd (r), Gyp, An
Solfatara	SOL16A	N40°49′35.1″ E14°8′30.9”	Altered materials near veins	Alu, Sm
	SOL16B	N40°49′35.1″ E14°8′30.9”	Altered materials near veins	Alu, Sm
	SOL16C	N40°49′35.1″ E14°8′30.9”	Altered materials near veins	Alu, Sm, Fe-ox
	SOL17	N40°49′35.5″ E14°8′32.4”	Altered materials near veins	Alu, Sm, S
	SOL22A	N40°49′37.7″ E14°8′30.8”	Mudpool	Sal, Rus, Am. Si
	SOL22B	N40°49′37.7″ E14°8′30.8”	Mudpool	Sal, Rus, Masc, S, Alg
	SOL22D	N40°49′37.7″ E14°8′30.8”	Mudpool	S, Alu, Ca
	BOC3	N40°43′19.3″ E13°52′46.4”	Protolith - Trachyte	Snd, Hb, Ilm
	SCA2	N40°42′14.0″ E13°51′40.3”	Protolith - Trachyte	Snd, Hb, Px, Musc
	FAN1A	N40°44′21.1″ E13°53′44.2”	Fumarole sublimate	Hal, Pick, Sm
Ischia	FAN1D	N40°44′21.1″ E13°53′44.2”	Hydrothermally altered materials	Alu, Kao, Qz
	FAN1G	N40°44′21.1″ E13°53′44.2”	Hydrothermally altered materials	Kao, Snd (r), Hal, Alum, Fe-ox
	FAN2B	N40°44′20.9″ E13°53′44.2”	Fumarole sublimate	Alg, Apj, Hal
	FAN3A	N40°44′21.0″ E13°53′44.3”	Hydrothermally altered materials	Alu, Kao, Qz, Snd (r)
	FAN3B	N40°44′21.0″ E13°53′44.3”	Hydrothermally altered materials	Alu, Kao, Qz, Snd (r)
	FAN4B	N40°44′21.4″ E13°53′44.7”	Hydrothermally altered materials	Kao, Alu, Snd (r)
	FAN4C	N40°44′21.4″ E13°53′44.7”	Hydrothermally altered materials	Kao, Alu, Snd (r)

Th, U, Sr and K are depleted. Sample CAL3 follows the same geochemical trend as CAL1, but less marked. Comparatively, the alunite rich CAL2 sample displays is depleted in Cs and Rb and enriched in Pb (Fig. 7a). Molybdenum and other chalcophile elements (i.e., Sb, Pb, Cu and Ga) are enriched compared to the protolith (see Supplementary data). CAL1 displays a distinct trend with depletions in REE and HREE/MREE fractionation. CAL2 exhibit a LREE/HREE fractionation. CAL3 shows a slight MREE/HREE fractionation (Fig. 7b).

The second assemblage patterns of La Calcara are similar in both trace elements and REE, with slight, albeit less pronounced fractionation (Fig. 7a, b). Compositions are like protolith values except for Cs and Rb which evolve in this assemblage. Sample CAL9 and 10 exhibits pronounced variations in trace elements compared to samples from the same assemblage as well as a slight LREE/HREE fractionation.

The trace element patterns of the third assemblage (labeled SCA - Fig. 3b) exhibit an evolution from the outer to the inner zones of the rounded breccia (from SCA1A to SCA1E), particularly noticeable in alkali elements (Fig. 7c). While they all follow a similar trend, SCA1B shows a slight depletion in trace elements and REE compared to other samples from this assemblage. HFSE remain largely consistent across samples (Fig. 7c). Lead is enriched in SCA1A, B, C, reaching up to 15, 3 and 30 times the average protolith composition, respectively (Fig. 7c, see Supplementary Data). REEs from the SCA assemblage exhibit an MREE/HREE fractionation, as well as a slight MREE/LREE fractionation, except sample SCA1E (core crystals). Profiles of SCA1A and C are similar, showing enrichment in LREE and MREE (up to Gd) and depletion in HREE. SCA1B, while slightly depleted in REE compared to other samples follows a similar trend to its neighbors. In contrast, the SCA1E profile is notably distinct, displaying a slight HREE/LREE fractionation and bulk REE enrichment compared to the average protolith (Fig. 7d).

4.2.2.3. Solfatara. Trace elements patterns of the Solfatara samples exhibit relatively depleted and serrated profiles (Fig. 7e). In the first assemblage (SOL16A, B, C, 17), which consist of alunite-rich samples, Th is slightly enriched, along with U and K. These samples are slightly depleted in Cs, Rb, Tl and Co (see Supplementary data). LREE are enriched up to 35 times the protolith composition (Fig. 7f).

SOL4 exhibits a depleted trend, albeit with values relatively close to the protolith in HFSE. SOL10 display similar trends less pronounced compared to the average protolith and a slight LREE/HREE fractionation is observed. SOL9 displays a similar trend as the first mineral assemblage but with an enrichment in REE and MREE/HREE fractionation.

Patterns from the third assemblage appear jagged and are globally depleted compared to the protolith and display opposite trends from the first assemblage. The REEs are also depleted, particularly in samples SOL22A and B (Fig. 7f), which are rich in salammoniac, mascagnite and russoite (Table 1). HFSE display similar compositions than the average protolith in every sample from La Solfatara.

4.2.2.4. Ischia. The first assemblage (comprising FAN1A, D, G) is characterized by serrated trace element profiles. Sample FAN01A (sublimate) displays slight enrichments in Ba, Th, U and REE (Fig. 7g). Samples FAN1D & G exhibit a depleted trace element profile, particularly evident in Cs, Rb, REE. Sample FAN1G shows Pb enrichment of up to 80 times (Fig. 7g). Sample FAN1A shows HREE/LREE fractionation

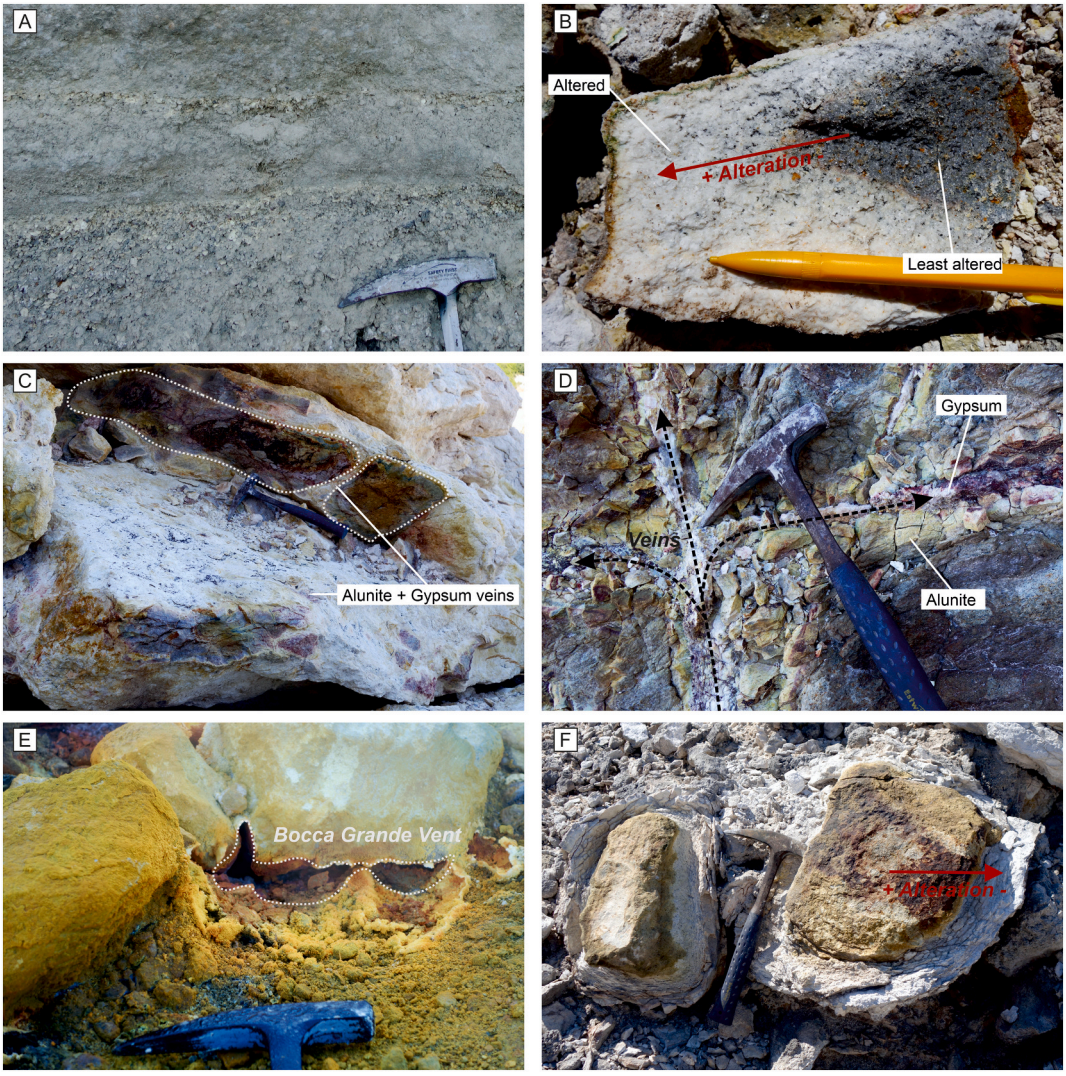

Fig. 4. Field pictures from Solfatara. (A) Primary tuff and pumices (NYT protolith). (B) Various alteration stages in brecciated lava: the white part on the edge is significantly altered while the greyish part is partially altered. (C & D) Hydrothermal breccia in altered lava where fractures (veins) are filled with alunite, gypsum and a small proportion of kaolinite. (E) Fumaroles Bocca Grande with native sulfur (F) Hydrothermal breccia with reacting white halos made of alunite.

and a slight positive Eu anomaly, while samples FAN1B and G show LREE/HREE fractionation and significant REE depletion. Notably, there is a positive Eu anomaly (Fig. 7h).

The patterns observed in the second assemblage (FAN2B, 3 A, 3B, 4B, 4C) closely reflect the protolith composition, albeit with slight depletions in Rb, Th and U (Fig. 7g). FAN2B display a similar trend as the FAN1A sample and a HREE/LREE fractionation. Sample FAN4C exhibits trace and REE patterns resembling those of the first assemblage, showing a depletion in REE and slight positive Eu anomaly (Fig. 7h).

4.3. Alteration indices

To compare the alteration products between the three sites, we used 11 indices to distinguish the studied hydrothermal systems from a geochemical perspective. Eight alterations indices from the literature (Table 3) are presented in this paper (see Supplementary data): Ishikawa Alteration Index (I-AI) (Ishikawa et al., 1976), Plagioclase Index of Alteration (PIA) (Fedo et al., 1995), Chlorite-Carbonate-Pyrite Index (CCPI) (Large et al., 2001), Chemical Index of Alteration (CIA) (Nesbitt and Young, 1982), Loss On Ignition (LOI), $\%SiO_2$ vs. $\%Al_2O_3$ and La/Yb. We also provide three new geochemical alteration indices based on our geochemical enrichment/depletion observations: La + Ce/Y, Zr + Hf/Ta + Nb, alkali / alkali-earth elements Sr + Ba/Cs + Rb.

The PIA value of fresh rocks is $\leq$60 and > 60 to 100 for altered rocks (Fedo et al., 1995). The I-AI ranges from 20 to 60 and from 60 to 100 for unaltered and hydrothermally altered rocks, respectively (Ishikawa et al., 1976). Our data show a separation between alkaline and calc-alkaline products, both protolith and alteration products as well as a clear increasing trend (Fig. 8a). The Al_2O_3 vs. SiO_2 plot (Fig. 8c) shows five different clusters. The first cluster includes the protoliths of the three systems. The second cluster comprises the alteration products from Ischia and Panarea, with significant kaolinite and clays in argillic alteration. The alunite samples define the third cluster (advanced argillic alteration) showing high Al_2O_3 contents and a significant depletion in silica compared with the protolith. Cluster 4 displays equal or slightly higher silica content while Al_2O_3 is depleted compared to the original protoliths. Cluster 5 includes products that deviate from the alteration trend. These samples were collected from fluid sublimates - efflorescence at the exit of the vents- with low Al_2O_3 and SiO_2 content. Alteration products tend to display high LOI (Fig. 8d) as clay minerals and sulfates are the main components of advanced argillic alteration zone and argillic alteration zone (see Table 1). The Loss on Ignition (LOI) of the sublimates is high, as they are mainly composed of hydrated minerals (Table 1). Chlorite-carbonate-pyrite index (CCPI) associated

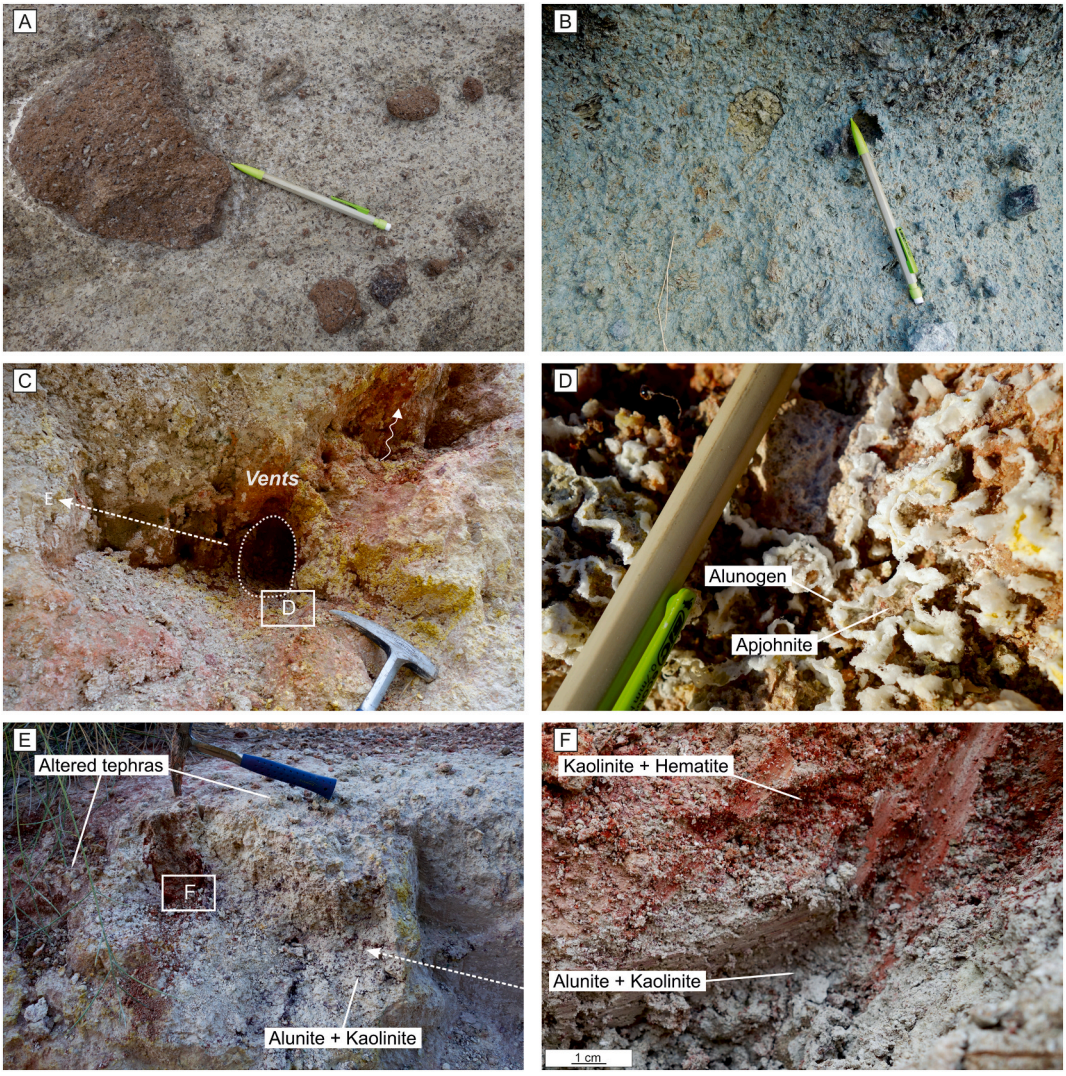

Fig. 5. Field pictures of the most representative Ischia samples. (A) Primary tuff rich in pumices and lapillis. (B) Altered tuff with altered tephras. (C) Altered tuff with mostly alunite and kaolinite. (D) Samples FAN 1F & 1E from Montagnone - Monte Cito (mostly alunite). (E) Mix of kaolinite and alunite close to the active vent in Monte Curvo. (F) Sample FAN 2B from Montagnone - Monte Cito close to fumaroles rich in alunogen and apjohnite.

with I-AI, it forms an alteration box plot that can link alteration products and geochemistry by providing, in our case, a qualitative estimate of the intensity of the feldspars and volcanic glass alteration (Large et al., 2001). Unlike I-AI, CCP Index is strongly affected by magmatic fractionation and the composition of primary volcanic rocks (Large et al., 2001) and alteration intensity.

5. Discussion

As highlighted in Fig. 8e, several alteration trends discriminate the alteration products of the different hydrothermal systems. For instance, alteration assemblages from fumaroles zones at Panarea show a clear drop in CCPI (10) and an average increase in I-AI (up to 60). On the other hand, andesitic breccia altered products show CCPI between 50 and 80 and I-AI increases significantly inward of the altered breccia.

5.1. Protolith heritage in alteration products

5.1.1. General geochemical behaviors

Alteration of volcanic rocks by hydrothermal processes is characterized by the leaching of major elements such as Fe, Na, Si, Mn, Mg, Ca and partly Al, K, Ti. In advanced argillitic alteration (mainly alunite + kaolinite), these elements, and HREE, are depleted compared to the protolith while Al, K, LREE, LILE are enriched. Rare earth elements, Al, Ti and Y show both immobile and mobile behavior depending on the different assemblages of alteration. HFSE have relatively immobile behavior. Various sites, generating acid sulfate alteration, such as Caldeiras-Furnas site (Bobos and Gomes, 2021), Sao Miguel Island (Azores Achipelago), Düvertepe district (Ece et al., 2013) - Simav Graben, Turkey) and Milos Island (Greece) are used here to discuss the alteration indices presented in Fig. 8.

The Panarea volcanic rocks and alteration products are different from those of Ischia and Solfatara as they have higher PIA and lower I-AI values (Fig. 8a). This difference is explained by the higher proportion of plagioclase (>50 %) in the Panarea protolith. Higher I-AI for alkaline protoliths indicates a lower CaO content and a comparatively higher K_2O compared to Panarea protolith. The alteration products follow a major alteration trendline, retaining their calc-alkaline or alkaline heritage, especially in Nb and Ta anomalies (Baier et al., 2008). We observe the same feature using the Zr + Hf/Ta + Nb trace element ratio - Fig. 8b - where the two domains are separated using Ta and Nb as proxies (Finlow-Bates and Stumpfl, 1981). It displays a split between protoliths and alteration products from calc-alkaline (Panarea) or alkaline (Solfatara & Ischia) environments (TAS diagram, Fig. 2a). Hence, the samples

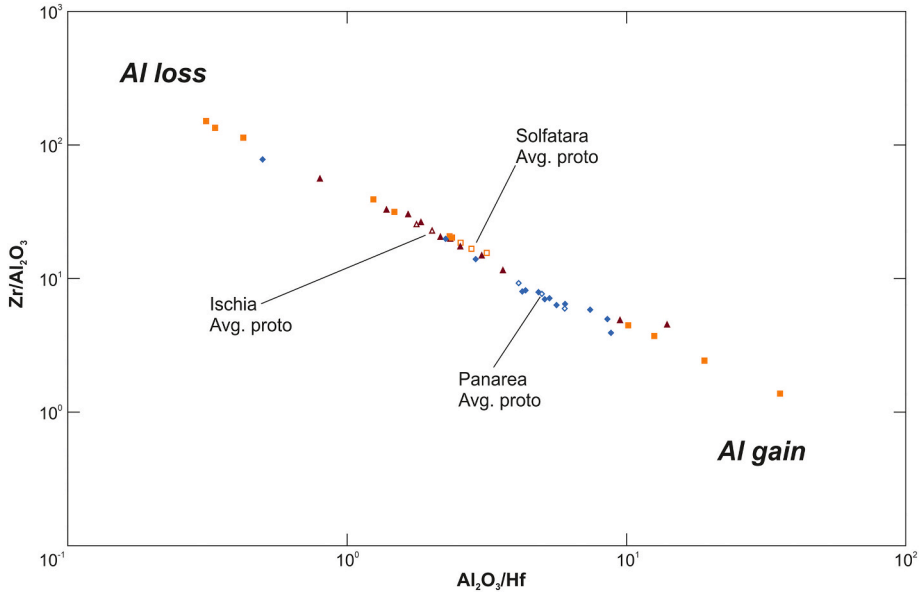

Fig. 6. Immobile element ratio for all samples collected in Panarea, La Sofatara and Ischia. Unfilled symbols are protoliths compositions. The mass gain/loss in Al during hydrothermal alteration creates a linear trend from the protolith clusters.

from Ischia and Solfatara samples are separated from Panarea, despite having similar mineralogy (alunite ± kaolinite).

This separation is also observed in other acid-sulfate alteration systems (Ece et al., 2013; Bobos and Gomes, 2021), such as Caldeiras-Furnas - Sao Miguel Island, Azores, alkaline - (Bobos and Gomes, 2021) and Düvertepe district - Simav Graben, Turkey, calc-alkaline - (Ece et al., 2013). Higher (La + Ce)/Y ratio differentiates the Solfatara alteration products from the other systems. Alunite is responsible for the fractionation of these elements (Fulignati et al., 1999; Karakaya, 2009; Inguaggiato et al., 2017, 2020). However, some samples from Panarea and Ischia containing alunite display similar lower (La + Ce)/Y ratios compared to Solfatara. The higher intensity processes taking place in the Solfatara hydrothermal system - steam-heated signature with magmatic-hydrothermal contributions (Piochi et al., 2015) - could result in higher fractionation of the REE. These alteration conditions control the fractionation of La, Ce and Y but have no or a slight influence on the fractionation of Ta, Zr, Hf and Nb.

During acid sulfate alteration, major elements are leached but most of the trace elements stay generally in the protolith (Mutlu et al., 2005). This intense cation leaching produces an increase in $(Al_2O_3)/(Na_2O + CaO + K_2O)$ ratio and favors alunite and kaolinite precipitation in a hot, acidic draining environment (Kadir et al., 2011). Thus, increasing LOI in association with Al + S + K content and decreasing SiO_2 content is a relevant indicator of kaolinization and alunitization (Kadir et al., 2022). However, alteration minerals such as alunite, kaolinite and smectites play a role in the fractionation of some elements (LILE, REE, etc.) from the protolith composition (Bobos and Gomes, 2021; Kadir et al., 2022). Other trace elements such as HFSE display similarities between protolith and alteration products (Fig. 6 - (Mutlu et al., 2005; Karakaya, 2009; Piochi et al., 2019; Bobos and Gomes, 2021). This could indicate a continuous process of exchange of chemical elements and complete in situ replacement of primary rock.

5.1.2. *Specific geochemical behaviors*

In addition to our interpretation about protolith heritage and alteration zones, some specific/local geochemical trends can be highlighted related to the different mineral assemblages. In the condensation of acid fluids zones, native sulfur could be derived from the cooling and oxidation of hydrothermal fluids upon contact with air at the fumarole exit (Africano and Bernard, 2000). Our data suggest that native sulfur, halotrichite, pickeringite, alunogen, apjohnite, salammoniac, russoite, coquimbite and mascagnite originate from the dense sulfurous vapor fluids condensing and cooling, with minor interactions with the protolith primary minerals. This statement is supported by (1) the disparate scattered distribution of these minerals in the geochemical patterns (Fig. 7) and alteration index graphs (Fig. 8), out of the major alteration trends highlighted between protoliths and alterites and (2) by the depleted geochemical signatures of these samples compared to the protolith. Slight or no protolith heritage is identified as those minerals are fluid derived.

CCPI vs I-AI and Sr + Ba/Cs + Rb vs La/Yb patterns display differences between the alteration products of hydrothermal breccias and fumaroles at Panarea (Fig. 8e, f). Kaolinite ± alunite are the main mineral phases and witness an advanced argillic alteration without residual primary minerals and alunite content decreasing away from active vents. Alunite-richer samples display lower CCPI and higher I-AI. Similar trends are observed in alunite and kaolinite from Düvertepe district (Ece et al., 2013). The enrichment in alteration products of Panarea in Mo, Sb, Pb, Ba and to a certain extent Ag and Zn suggests two possible explanations: (1) a higher fluid temperature favoring metal transport such in sulfides hosted environment or in low sulfidation epithermal metal-bearing deposits (Cheynet et al., 2000; Grosche et al., 2023 and Fig. 9); (2) alteration of sulfides such as pyrite (Fig. 3e, f) – those metals being trace elements in pyrite - and galena/sphalerite, also observed in the neighborhood of these alterations (Savelli et al., 1999; Dekov et al., 2013; Piochi et al., 2015, 2019). It seems that those metals were transported from an external source by hydrothermal solutions (Çelik Karakaya et al., 2021).

On the other hand, the altered andesitic breccia shows clear evolution over CCPI and I-AI indices from the inside to the outside of the altered breccia. In this environment, the protolith is mainly replaced by kaolinite (Barrett and Joseph, 2018). Leaching of Na, Ca, Mg, Fe, LILE, REE by the fluids could precipitate kaolinite and then smectite as the pH increases (Ece et al., 2013). The Sr + Ba/Cs + Rb ratio (Fig. 8f) shows a difference between protolith and altered andesitic breccia, due to the low Sr and Ba enrichment and the depletion in Cs and Rb in the kaolinitic assemblage.

All Solfatara samples, except for sublimates, show a similar trend, with a significant increase in I-AI >90 and a sharp drop in CCPI <20 compared to the trachy-andesitic protolith, towards the lower right

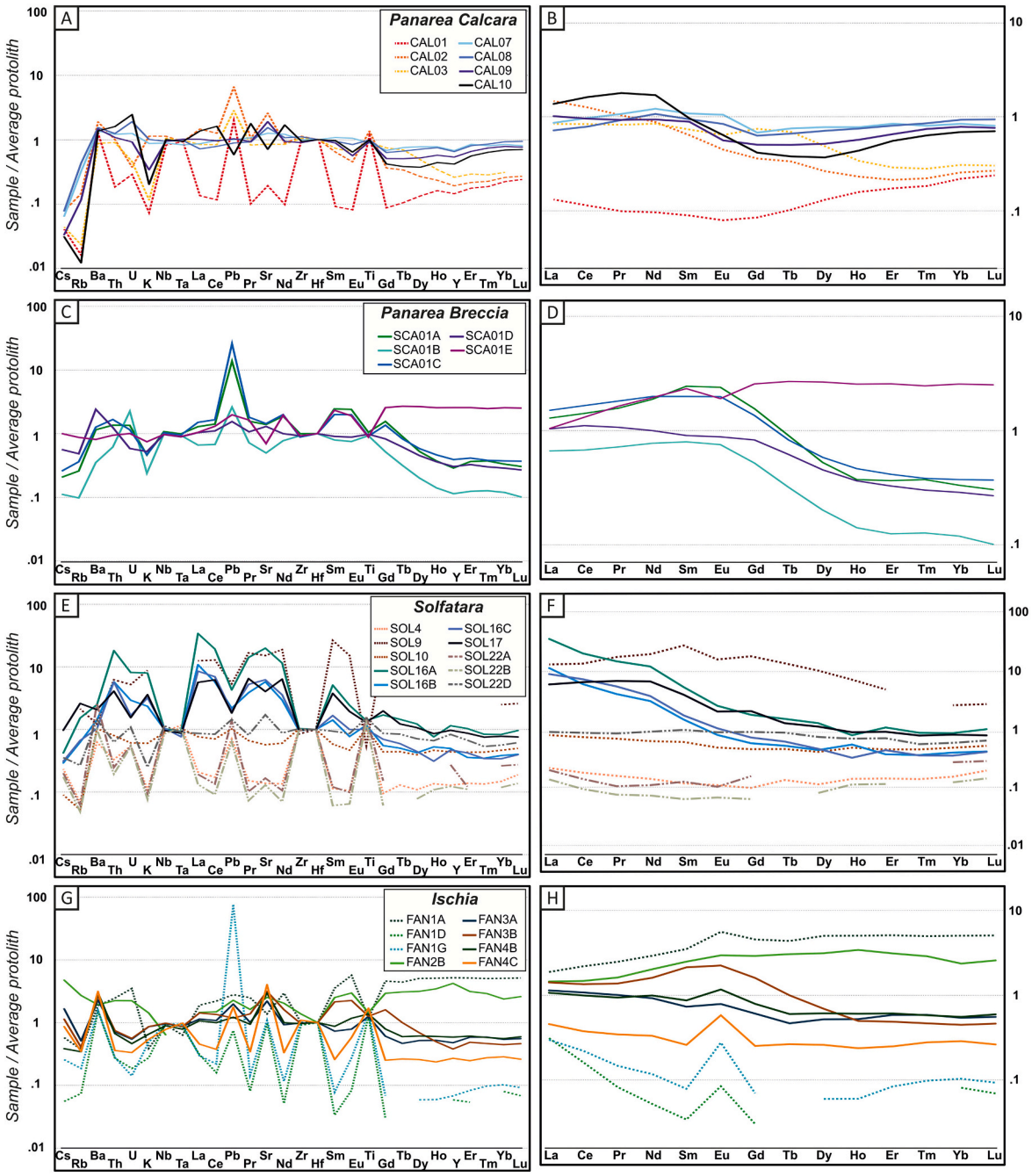

Fig. 7. Reconstructed compositions of trace and REE elements patterns of alteration products normalized to average protolith composition.

corner of the graph corresponding to the K-feldspar pole. All samples are alunite-bearing and heavily altered. No residual primary minerals were identified. This trend is even more pronounced than in the Panarea alunitic samples. Alunite from Düvertepe district (Ece et al., 2013) displays the same trend. But the trend is different for Ischia, with an increase in CCPI and I-AI compared with the trachytic protolith. This trend is explained by the occurrence of residual sanidine but mainly by a lower intensity of alteration than in Solfatara fumaroles (Piochi et al., 2015, 2019). However, the alteration trend observed in the Sr + Ba/Cs + Rb vs La/Yb plot (Fig. 7f) shows similar alteration patterns between the three sampling sites. It shows LREE/HREE fractionation (various magnitudes), low Sr and Ba enrichment and depletion in Cs and Rb during alteration. These parameters seem to indicate preferential alteration of feldspars (plagioclase and K-feldspar).

5.2. *Fluid-protolith interactions in alunite and kaolinite formation model*

5.2.1. *Constrains from the alunite and kaolinite formation*

In Panarea, alunite is ubiquitous in fumarole patches (Fig. 3c). Amorphous silica is often found in association with alunite where acidic conditions and high temperature prevail (silicification – Fig. 9a). The protolith alteration leads to mobilization of Al, Ca, Na, Fe and Mg (Africano and Bernard, 2000). Some amorphous silica inclusions can be found associated with alunite attesting relative Si mobility at low pH and high temperature and silica excess. In addition, fumaroles are surrounded by large patches of argillic type alteration (Fig. 9b) containing (alunite), kaolinite and smectite in altered andesitic prisms (replacement of the protolith, Fig. 3b) while gypsum and kaolinite seal the hydrothermal veins (veins-type in open cavities – Fig. 3e). Thereby, the mineralogical and geochemical changes observed inward the altered

Table 3
Chemical indices of alteration, their formula, and references.

Alteration index	Formula	Reference	Use
Ishikawa Alteration Index (I-AI)	$\frac{K_2O + MgO}{MgO + CaO + Na_2O + K_2O} * 100$	(Ishikawa et al., 1976)	Increase with alteration Fresh rocks <60 Altered rocks >60
Plagioclase Index of Alteration (PIA)	$\frac{Al_2O_3 - K_2O}{Al_2O_3 + CaO + Na_2O + K_2O} * 100$	(Fedo et al., 1995)	Increase with alteration Fresh rocks <60 Altered rocks >60
Chlorite-Carbonate-Pyrite Index (CCPI)	$\frac{MgO + FeO}{MgO + FeO + Na_2O + K_2O} * 100$	(Large et al., 2001)	Quantitative estimation of alteration intensity - zonation
Chemical Index of Alteration (CIA)	$\frac{Al_2O_3}{Al_2O_3 + CaO + Na_2O + K_2O} * 100$	(Nesbitt and Young, 1982)	Increase with alteration Fresh rocks <60 Altered rocks >60

protolith (Fig. 3b, Fig. 7a,b) reflect interactions between fluids and andesitic prisms. The mineral assemblage evolves inward from (alunite) - kaolinite (Fig. 3b, sample SCA01A-B) to kaolinite + smectites + iron oxides (Fig. 3b, sample SCA01C) to smectite + residual plagioclases, pyroxenes and quartz. The core of the altered andesitic prisms (argillic type alteration; Fig. 9c) shows macrocrysts of plagioclase and hornblende (Fig. 3b, sample SCA01D-E). This highlights that acid solutions play a key role in the mobilization of some chemical elements and are evolving during their reactions with the protolith by neutralizing (Ece et al., 2013) leading to the precipitation of these late minerals such as smectite and Fe oxides (Barrett and Joseph, 2018). The hydrothermal system of Panarea is distinguished by a high water/rock ratio and a high rate of seawater circulation (Italiano and Nuccio, 1991). Besides, halite is also found associated with late hydrothermal veins and veinlets.

However, in La Solfatara, alunite is more abundant than kaolinite (Piochi et al., 2015) and referred to as "solfataric-type" alteration (Fig. 9a, b). Fluids stay in acidic conditions with a high activity of $[SO_4]^{2-}$ leading to acid sulfate zones. This mineralogy suggests complex acidic sulfate conditions of fluids and sulfur precipitations from H_2S emissions. Therefore, crystallization of alunite is favored. A small amount of kaolinite crystallizes when pH increases due to acid neutralization by interaction with the protolith minerals. Equilibrium between alunite and kaolinite requires a significant H_2SO_4 concentration, while prevailing alunite alteration products involve atmospheric oxidation of H_2S into H_2SO_4 (Mutlu et al., 2005). If pH increases, kaolinite remains stable over alunite under the same SO_4 and K^+ activities (Mayer et al., 2016). Moreover, in the Saphane deposit, alunite is dominant because it might be formed above the water table where atmospheric oxygen could oxidize H_2S to H_2SO_4 (Mutlu et al., 2005). Smectite and alunite coexist in Solfatara suggesting different fluid conditions (Fig. 9b, c). Smectite, (gypsum), and alunite are sealing the hydrothermal breccia veins and are found in mudpools (Fig. 4f). In Solfatara, ascending magmatic fluids mix with meteoric waters with an average proportion (1983–2006 period) of ~1:4 magmatic fluids and ~ 3/4 hot hydrothermal waters (Caliro et al., 2007). Above this mixing zone, hydrothermal fluids dominate and favor reduced gases such as NH_4 and H_2S while oxidant magmatic gases such as SO_2, HCl, HF are typical below the mixing zone (Fig. 9a), at higher temperatures (Caliro et al., 2007). Smectite and gypsum could have crystallized during mixing of hydrothermal fluids and meteoric waters or around the acid sulfate zone, where activity is lower (Piochi et al., 2019).

Yet, in Ischia, alunite and kaolinite are the two most abundant alteration minerals. The most common assemblage in active fumaroles zones is (amorphous) silica – (halotrichite - alunogen) alunite – kaolinite. Alunite, alunogen and kaolinite indicate acid conditions with a pH around 4–5, while halotrichite refers to pH <2 (Piochi et al., 2019). Those advanced argillic alteration facies in the Montagnone - Monte Cito reflect acid sulfate conditions (Fig. 9a). The magmatic gas contribution in Monte Cito from a deep reservoir seems clear, based on the high $^3He/^4He$ ratios, CO_2 enrichment and H_2S occurrence (Di Napoli et al., 2009; Piochi et al., 2019). Large amount of heat discharge occurs alongside faults and fractures mainly on the western and southern parts of the volcano-tectonic resurgence of Mt. Epomeo (Carlino et al., 2014). The magmatic contribution is high in the Montagnone – Monte Cito facies, inducing the precipitation of S-bearing minerals such as halotrichite, pickeringite, alunogen, apjohnite and native S from the sulfurous vapor fluids. Pervasive acid and hot fluids are infilling through cracks and faults of the protolith – mainly tuffs and pumices – and reacting in situ with the walls. They also infill the porosity and permeability, enlarging the reaction and alteration processes over time. Alunite and kaolinite are formed by reaction between those fluids and the protolith as replacement deposits (Fig. 9b). In this system, no vein-type deposit was observed because the fluids infilled the tuff and pumices through their porosity.

5.2.2. *Partitioning of REE in alunite and kaolinite*

LREE are generally enriched in alunite, whereas HREE are depleted compared to the protolith (Fig. 7). Alunite is known to scavenge LREE over HREE, probably due to the ionic radius differences (Fulignati et al., 1999; Karakaya, 2009; Inguaggiato et al., 2017). Moreover, studies of the acidic waters from those hydrothermal systems show a LREE depletion over HREE, which is explained by alunite precipitation (Inguaggiato et al., 2017, 2020). In our dataset, alunite from Solfatara has a higher LREE/HREE fractionation regarding to the local protolith normalization than alunite from Panarea and Ischia. This could be due to the higher REE content of the protolith in Solfatara, supporting the hypothesis of a protolith heritage and a geochemical control in the secondary minerals or by differences in the physico-chemical conditions of the fluids/rocks interactions.

However, alunite, as well as kaolinite, from Ischia shows slight or no LREE/HREE fractionation despite similar REE composition in the protolith. The composition of the alunite and kaolinite from Ischia is strongly correlated to that of the protolith with only minor enrichments/depletion (Fig. 7f, h) and subparallel patterns. This could be explained by the early precipitation of halotrichite and alunogen before alunite and kaolinite or different alteration conditions. These minerals could carry some REE before alunite and kaolinite formation. Therefore, alunite and kaolinite are deprived of some REE, showing no or slight fractionation of REE.

Yet, we observe the same behavior in Solfatara, with precipitated alunite precursor minerals and a similar protolith (Fig. 2, Fig. 9). The patterns of alunite at Solfatara clearly show a significant fractionation of the REEs in alunite. The fractionation would therefore be effective at the mineralogical level but also at the level of the physico-chemical conditions of the fluids. Either the Solfatara alunite precursor minerals do not trap REEs, or REEs behave differently depending on the fluids that interact with the protolith. The first hypothesis seems inappropriate according to the mineralization identified. Therefore, the shape of the REE pattern is mainly controlled by mineralogy but also on their valence state, the temperature, Eh/pH conditions and potential ligands of the fluids (Karakaya, 2009).

Alunite and kaolinite can be associated, as shown by many studies in similar environments, and might display similar geochemical trends (Mutlu et al., 2005; Kadir et al., 2011, 2022; Ece et al., 2013; Çelik Karakaya et al., 2021; Bobos and Gomes, 2021). In Panarea, as shown by our results and alteration indices patterns (Fig. 7a, c, Fig. 8c, e, f), kaolinite-rich samples can exhibit two different geochemical behaviors.

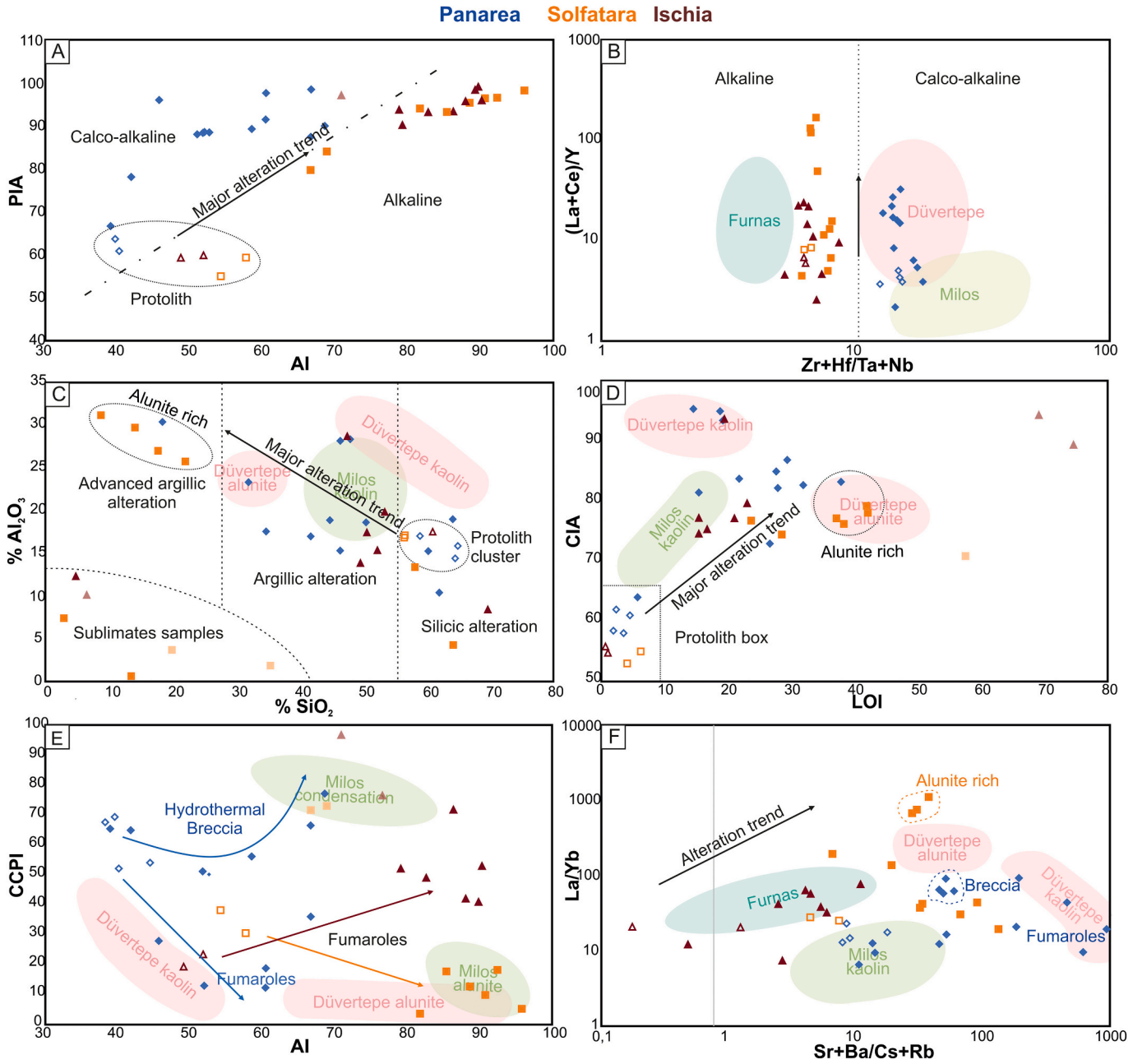

Fig. 8. Chemical weathering indices and elementary ratios for the protolithic and altered samples from Solfatara, Ischia and Panarea. Some sublimate samples are out of the scale. (A) PIA vs. I-AI (B) (La + Ce)/Y vs. Zr + Hf/Ta + Nb (C) Al_2O_3 vs. SiO_2 (D) CIA vs. LOI (E) CCPI vs. I-AI and (F) La/Yb vs. Mobile elements ratio Sr + Ba/Cs + Rb. Clustered data are from (Ece et al., 2013; Bobos and Gomes, 2021). Labeled symbols without clusters are presented in the Supplementary data.

However, both profiles are similar to the REE and trace element values of the protolith. This could indicate two types of kaolinite at Panarea. Type 1 kaolinite shows slight (or no) enrichment/depletion compared to local protolith except LILE, occurring alongside alunite. This type of kaolin with specific geochemical behaviors is found near the active fumaroles. Type 2 kaolinite shows higher MREE/HREE fractionation with HREE depletion compared to the protolith. Type 2 may have formed under high fluid/rock interactions and higher pH allowing kaolinite precipitation (unsignificant alunite content) than close to active fumaroles. In Type 2 kaolinite, enrichments in chalcophiles elements are spotted compared to the protolith. Ionic strength, crystallinity and pH also control sorption and fractionation of REE in kaolinite (Yang et al., 2019). In Ischia, kaolinite rich samples collected nearby the active fumaroles display a similar REE behavior than type 1 kaolinite in Panarea (Fig. 7f, h).

6. Conclusion

This paper provides mineralogical assemblages used to identify the geochemical behavior of the various alteration products at Panarea (Aeolian Islands), Ischia and La Solfatara (Phlegrean Fields) by monitoring the hydrothermal alteration with alteration indices. Global alteration zones and geochemical behaviors have been highlighted while, on a local scale, some differences between the hydrothermal systems can be established.

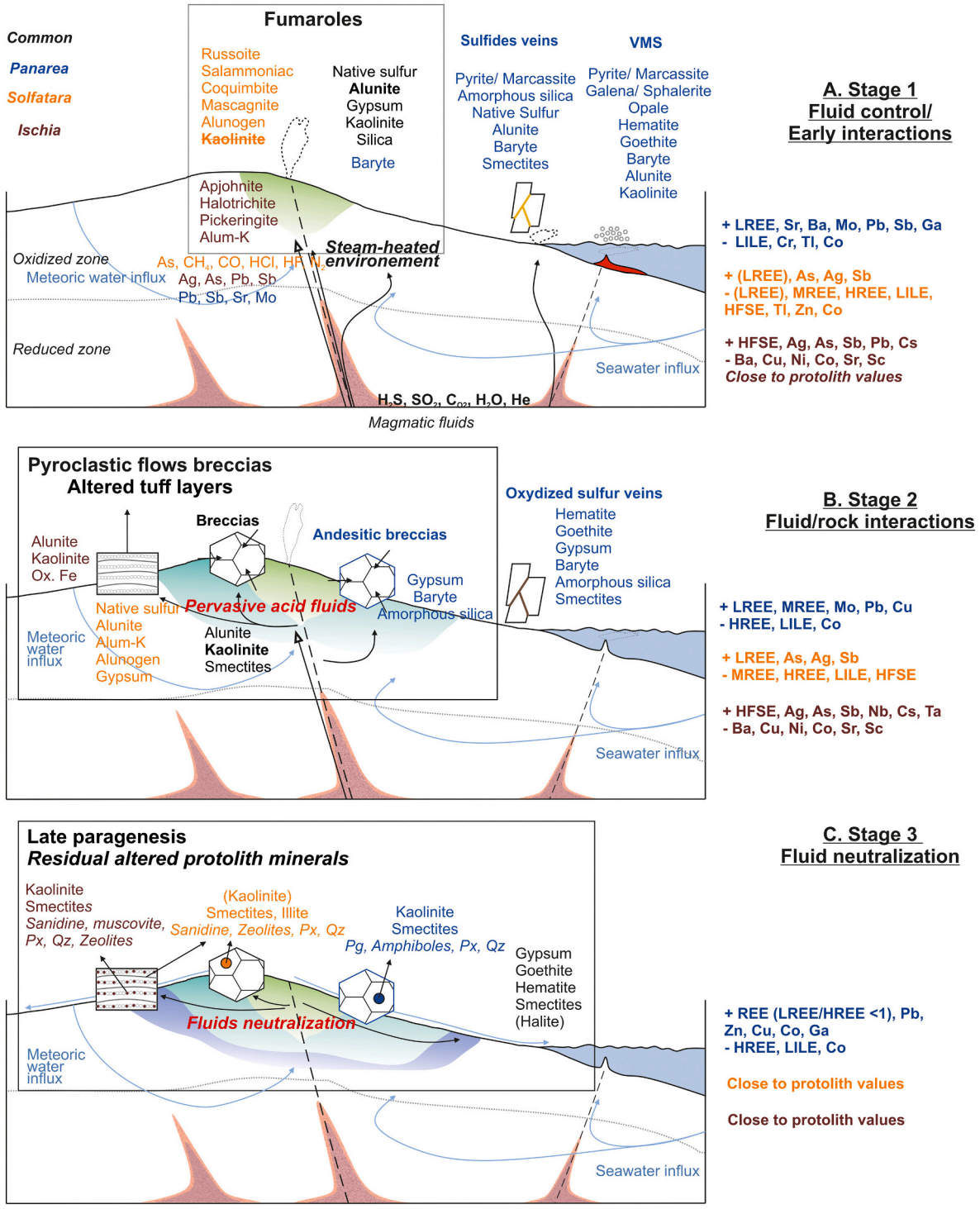

Fig. 9. Integrated model of the hydrothermal alterations and new paragenesis occurring in the studied areas in a mineralogical/geochemical point of view. Stage 1 corresponds to fluid control/early surface interactions with protolith. Stage 2 characterizes the rock/fluids interactions generated by the pervasive acid fluids and their progressive neutralization/precipitation. Stage 3 illustrates the mineralogy and geochemistry triggered by the neutralization of fluids in the protolith. The scale is not accurate.

1. Some weathering indices such as CIA, PIA and AI can monitor the intensity of hydrothermal alterations in Panarea, Ischia and La Solfatara.
2. There is a significant protolith heritage in all altered samples, except for condensation products directly coming from the inside of the vents. Trace elements content of the protolith and alteration products are similar and could indicate a process of exchange of chemical elements by a complete-partial in situ replacement of primary rock. Alteration products retain their Nb and Ta calc-alkaline or alkaline heritage.
3. There is an alkali elements loss during hydrothermal alteration.
4. Different intensities of alteration and geochemical behaviors are occurring despite a similar mineralogy in La Solfatara, Panarea and Ischia, hinting local vs. global geochemical behaviors.
5. Alunite crystallization induces a LREE/HREE fractionation. LREE are generally enriched while HREE are depleted compared to the

protolith. Multi-type kaolinite also plays a role in the REE fractionation. It could be appropriate to perform a detailed geochemical study of multiple kaolinites within the sampled locations.

6. Acid fluids significantly mobilize REE during the interaction with protolith. Moreover, REE concentration is governed by the protolith composition; the fractionation between LREE, MREE and HREE is controlled by the protolith composition, the alteration intensity and mineralogy, pH, ionic strength and possibly crystallinity of alteration minerals.

CRediT authorship contribution statement

Théo Bouvart: Writing – original draft, Project administration, Methodology, Investigation, Data curation, Conceptualization. **Julien Poot:** Writing – review & editing, Writing – original draft, Investigation, Data curation, Conceptualization. **Augustin Dekoninck:** Writing – review & editing, Investigation, Conceptualization. **Flore Schmit:** Investigation. **Maxime Keutgen De Greef:** Writing – review & editing, Data curation. **Jacqueline Vander Auwera:** Writing – review & editing. **Alain Bernard:** Writing – review & editing. **Johan Yans:** Writing – review & editing, Validation, Supervision, Resources, Project administration, Investigation, Conceptualization.

Funding source

This research did not receive any specific grant from funding agencies in the public, commercial, or not-for-profit sectors.

Declaration of competing interest

The authors declare that they have no known competing financial interests or personal relationships that could have appeared to influence the work reported in this paper.

Acknowledgements

Our warmest thanks go to Gaëtan Rochez (UNamur) and Nicolas Delmelle (ULiège) for their support during sample preparation and X-ray processing.

Appendix A. Supplementary data

Supplementary data to this article can be found online at https://doi.org/10.1016/j.chemer.2024.126204.

Data availability

Most data is included in the supplementary file. More data will be made available on request.

References

Acocella, V., Funiciello, R., 1999. The interaction between regional and local tectonics during resurgent doming: the case of the island of Ischia, Italy. J. Volcanol. Geotherm. Res. 88, 109–123. https://doi.org/10.1016/S0377-0273(98)00109-7.

Africano, F., Bernard, A., 2000. Acid alteration in the fumarolic environment of Usu volcano, Hokkaido, Japan. J. Volcanol. Geotherm. Res. 475–495.

Baier, J., Audétat, A., Keppler, H., 2008. The origin of the negative niobium tantalum anomaly in subduction zone magmas. Earth Planet. Sci. Lett. 267, 290–300. https://doi.org/10.1016/j.epsl.2007.11.032.

Barrett, T.J., Joseph, E.P., 2018. Extreme alteration in an acid-sulphate geothermal field: Sulphur Springs, Saint Lucia. Chem. Geol. 500, 103–135. https://doi.org/10.1016/j.chemgeo.2018.09.028.

Bobos, I., Gomes, C., 2021. Mineralogy and geochemistry (HFSE and REE) of the present-day acid-sulfate types alteration from the active hydrothermal system of Furnas volcano, São Miguel Island. The Azores Archipelago. Minerals 11, 335. https://doi.org/10.3390/min11040335.

Boyce, A.J., Fulignati, P., Sbrana, A., Fallick, A.E., 2007. Fluids in early stage hydrothermal alteration of high-sulfidation epithermal systems: a view from the Vulcano active hydrothermal system (Aeolian Island, Italy). J. Volcanol. Geotherm. Res. 166, 76–90. https://doi.org/10.1016/j.jvolgeores.2007.07.005.

Brown, R.J., Civetta, L., Arienzo, I., et al., 2014. Geochemical and isotopic insights into the assembly, evolution and disruption of a magmatic plumbing system before and after a cataclysmic caldera-collapse eruption at Ischia volcano (Italy). Contrib. Mineral. Petrol. 168, 1–23. https://doi.org/10.1007/s00410-014-1035-1.

Calanchi, N., Peccerillo, A., Tranne, C.A., et al., 2002. Petrology and geochemistry of volcanic rocks from the island of Panarea: implications for mantle evolution beneath the Aeolian island arc (southern Tyrrhenian Sea). J. Volcanol. Geotherm. Res. 115, 367–395. https://doi.org/10.1016/S0377-0273(01)00333-X.

Caliro, S., Chiodini, G., Moretti, R., et al., 2007. The origin of the fumaroles of La Solfatara (Campi Flegrei, South Italy). Geochim. Cosmochim. Acta 71, 3040–3055. https://doi.org/10.1016/j.gca.2007.04.007.

Capaccioni, B., Tassi, F., Vaselli, O., et al., 2007. Submarine gas burst at Panarea Island (southern Italy) on 3 November 2002: a magmatic versus hydrothermal episode. J. Geophys. Res. Solid Earth 112, B05201. https://doi.org/10.1029/2006JB004359.

Carlino, S., Somma, R., Troiano, A., et al., 2014. The geothermal system of Ischia Island (southern Italy): critical review and sustainability analysis of geothermal resource for electricity generation. Renew. Energy 62, 177–196. https://doi.org/10.1016/j.renene.2013.06.052.

Casalini, M., Avanzinelli, R., Heumann, A., De Vita, S., Sansivero, F., Conticelli, S., Tommasini, S., 2017. Geochemical and radiogenic isotope probes of Ischia volcano, Southern Italy: Constraints on magma chamber dynamics and residence time. American Mineralogist 102 (2), 262–274. https://doi.org/10.2138/am-2017-5724.

Çelik Karakaya, M., Karakaya, N., Temel, A., Yavuz, F., 2021. Mineralogical and geochemical properties and genesis of kaolin and alunite deposits SE of Aksaray (Central Turkey). Appl. Geochem. 124, 104830. https://doi.org/10.1016/j.apgeochem.2020.104830.

Cheynet, B., Dall'Aglio, M., Garavelli, A., et al., 2000. Trace elements from fumaroles at Vulcano Island (Italy): rates of transport and a thermochemical model. J. Volcanol. Geotherm. Res. 95, 273–283. https://doi.org/10.1016/S0377-0273(99)00122-5.

Chiodini, G., Caliro, S., Caramanna, G., et al., 2006. Geochemistry of the submarine gaseous emissions of Panarea (Aeolian Islands, southern Italy): magmatic vs. hydrothermal origin and implications for volcanic surveillance. Pure Appl. Geophys. 163, 759–780. https://doi.org/10.1007/s00024-006-0037-y.

Chiodini, G., Avino, R., Caliro, S., Minopoli, C., 2011. Temperature and pressure gas geoindicators at the Solfatara fumaroles (Campi Flegrei). Ann. Geophys. 54, 151–160.

Chiodini, G., Vandemeulebrouck, J., Caliro, S., et al., 2015. Evidence of thermal-driven processes triggering the 2005–2014 unrest at Campi Flegrei caldera. Earth Planet. Sci. Lett. 414, 58–67. https://doi.org/10.1016/j.epsl.2015.01.012.

Chiodini, G., Caliro, S., Avino, R., et al., 2021. Hydrothermal pressure-temperature control on CO2 emissions and seismicity at Campi Flegrei (Italy). J. Volcanol. Geotherm. Res. 414, 107245. https://doi.org/10.1016/j.jvolgeores.2021.107245.

Chiodini, G., Caliro, S., Avino, R., et al., 2022. The hydrothermal system of the Campi Flegrei caldera, Italy. In: Orsi, G., D'Antonio, M., Civetta, L. (Eds.), Springer. Berlin Heidelberg, Berlin, Heidelberg, pp. 239–255.

Colella, A., Di Benedetto, C., Calcaterra, D., et al., 2017. The Neapolitan yellow tuff: an outstanding example of heterogeneity. Constr. Build. Mater. 136, 361–373. https://doi.org/10.1016/j.conbuildmat.2017.01.053.

Crisci, G.M., De Francesco, A.M., Mazzuoli, R., et al., 1989. Geochemistry of recent volcanics of Ischia Island, Italy: evidences for fractional crystallization and magma mixing. Chem. Geol. 78, 15–33. https://doi.org/10.1016/0009-2541(89)90049-1.

Dekov, V.M., Kamenov, G.D., Abrasheva, M.D., et al., 2013. Mineralogical and geochemical investigation of seafloor massive sulfides from Panarea platform (Aeolian arc, Tyrrhenian Sea). Chem. Geol. 335, 136–148. https://doi.org/10.1016/j.chemgeo.2012.10.048.

Di Giuseppe, M.G., Troiano, A., Fedele, A., et al., 2015. Electrical resistivity tomography imaging of the near-surface structure of the Solfatara crater, Campi Flegrei (Naples, Italy). Bull. Volcanol. 77. https://doi.org/10.1007/s00445-015-0910-6.

Di Napoli, R., Aiuppa, A., Bellomo, S., et al., 2009. A model for Ischia hydrothermal system: evidences from the chemistry of thermal groundwaters. J. Volcanol. Geotherm. Res. 186, 133–159. https://doi.org/10.1016/j.jvolgeores.2009.06.005.

Di Vito, M.A., Isaia, R., Orsi, G., et al., 1999. Volcanism and deformation since 12,000 years at the Campi Flegrei caldera (Italy). J. Volcanol. Geotherm. Res. 91, 221–246. https://doi.org/10.1016/S0377-0273(99)00037-2.

Doherty, A.L., Cannatelli, C., Raia, F., Belkin, H.E., Albanese, S., Lima, A., De Vivo, B., 2015. Geochemistry of selected lavas of the Panarea volcanic group. Aeolian Arc, Italy. Mineralogy and Petrology 109 (5), 597–610. https://doi.org/10.1007/s00710-015-0385-3.

Ece, Ö.I., Ekinci, B., Schroeder, P.A., et al., 2013. Origin of the Düvertepe kaolin-alunite deposits in Simav graben, Turkey: timing and styles of hydrothermal mineralization. J. Volcanol. Geotherm. Res. 255, 57–78. https://doi.org/10.1016/j.jvolgeores.2013.01.012.

Fedo, C.M., Wayne Nesbitt, H., Young, G.M., 1995. Unraveling the effects of potassium metasomatism in sedimentary rocks and paleosols, with implications for paleoweathering conditions and provenance. Geology 23, 921. https://doi.org/10.1130/0091-7613(1995)023<0921:UTEOPM>2.3.CO;2.

Finlow-Bates, T., Stumpfl, E.F., 1981. The behaviour of so-called immobile elements in hydrothermally altered rocks associated with volcanogenic submarine-exhalative ore deposits. Mineral. Deposita 16, 319–328. https://doi.org/10.1007/BF00202743.

Fulignati, P., Gioncada, A., Sbrana, A., 1999. Rare-earth element (REE) behaviour in the alteration facies of the active magmatic-hydrothermal system of Vulcano (Aeolian Islands, Italy). J. Volcanol. Geotherm. Res. 88, 325–342. https://doi.org/10.1016/S0377-0273(98)00117-6.

Grosche, A., Klemd, R., Denkel, K., Keith, M., Haase, K.M., Voudouris, P.C., Alfieris, D., Wiedenbeck, M., 2023. Sources, transport, and deposition of metal(loid)s recorded by sulfide and rock geochemistry: constraints from a vertical profile through the epithermal Profitis Ilias Au prospect, Milos Island, Greece. Mineralium Deposita 58 (6), 1101–1122. https://doi.org/10.1007/s00126-023-01170-2.

Heap, M.J., Baumann, T., Gilg, H.A., et al., 2021. Hydrothermal alteration can result in pore pressurization and volcano instability. Geology 49, 1348–1352. https://doi.org/10.1130/G49063.1.

Inguaggiato, C., Burbano, V., Rouwet, D., Garzón, G., 2017. Geochemical processes assessed by rare earth elements fractionation at "Laguna Verde" acidic-sulphate crater lake (Azufral volcano, Colombia). Appl. Geochem. 79, 65–74. https://doi.org/10.1016/j.apgeochem.2017.02.013.

Inguaggiato, C., Pappaterra, S., Peiffer, L., et al., 2020. Mobility of REE from a hyperacid brine to secondary minerals precipitated in a volcanic hydrothermal system: Kawah Ijen crater lake (Java, Indonesia). Sci. Total Environ. 740, 140133. https://doi.org/10.1016/j.scitotenv.2020.140133.

Ishikawa Y, Sawaguchi T, Iwaya S, Horiuchi M (1976) Deliniation of prospecting targets for Kuroko deposits based on modes of volcanism of underlying dacite and alteration halos (in Japanese with English abs.). Mining Geol. 26:206–117.

Italiano, F., Nuccio, P.M.M., 1991. Geochemical investigations of submarine volcanic exhalations to the east of Panarea, Aeolian Islands, Italy. J. Volcanol. Geotherm. Res. 46, 125–141. https://doi.org/10.1016/0377-0273(91)90079-F.

Kadir, S., Erman, H., Erkoyun, H., 2011. Mineralogical and geochemical characteristics and genesis of hydrothermal kaolinite deposits within neogene volcanites, Kütahya (western Anatolia), Turkey. Clay Clay Miner. 59, 250–276. https://doi.org/10.1346/CCMN.2011.0590304.

Kadir, S., Ateş, H., Erkoyun, H., et al., 2022. Genesis of alunite-bearing kaolin deposit in Mudamköy member of the Miocene Göbel formation, Mustafakemalpaşa (Bursa). Turkey. Appl. Clay Sci. 221, 106407. https://doi.org/10.1016/j.clay.2022.106407.

Karakaya, N., 2009. REE and HFS element behaviour in the alteration facies of the Erenler Dağı Volcanics (Konya, Turkey) and kaolinite occurrence. J. Geochem. Explor. 101, 185–208. https://doi.org/10.1016/j.gexplo.2008.07.001.

Large, R.R., Gemmell, J.B., Paulick, H., Huston, D.L., 2001. The alteration box plot: a simple approach toUnderstanding the relationship between alteration mineralogy andLithogeochemistry associated with volcanic-hosted massive sulfide deposits. Econ. Geol. 96, 957–971. https://doi.org/10.2113/gsecongeo.96.5.957.

Le Bas, Le Maitre, Streckeisen, A., Zanettin, B., Bas, M.J.L., Maitre, R.W.L., Streckeisen, A., Zanettin, B., 1986. A chemical classification of volcanic rocks based on the total alkali-silica diagram. J. Petrol. 27 (3), 745–750. https://doi.org/10.1093/petrology/27.3.745.

Lucchi, F., Tranne, C.A., Peccerillo, A., et al., 2013. Geological history of the panarea volcanic group (eastern aeolian archipelago). Geol. Soc. Mem. 37, 351–395. https://doi.org/10.1144/M37.12.

MacLean, W.H., 1990. Mass change calculations in altered rock series. Mineral. Deposita 25, 44–49. https://doi.org/10.1007/BF03326382.

Mayer, K., Scheu, B., Montanaro, C., et al., 2016. Hydrothermal alteration of surficial rocks at Solfatara (Campi Flegrei): Petrophysical properties and implications for phreatic eruption processes. J. Volcanol. Geotherm. Res. 320, 128–143. https://doi.org/10.1016/j.jvolgeores.2016.04.020.

Mutlu, H., Sariiz, K., Kadir, S., 2005. Geochemistry and origin of the Şaphane alunite deposit, Western Anatolia, Turkey. Ore Geol. Rev. 26, 39–50. https://doi.org/10.1016/j.oregeorev.2004.12.003.

Nesbitt, H.W., Young, G.M., 1982. Early proterozoic climates and plate motions inferred from major element chemistry of lutites. Nature 299, 715–717. https://doi.org/10.1038/299715a0.

Orsi, G., De Vita, S., Di Vito, M., 1996. The restless, resurgent Campi Flegrei nested caldera (Italy): constraints on its evolution and configuration. J. Volcanol. Geotherm. Res. 74, 179–214. https://doi.org/10.1016/S0377-0273(96)00063-7.

Orsi, G., Civetta, L., Del Gaudio, C., et al., 1999. Short-term ground deformations and seismicity in the resurgent Campi Flegrei caldera (Italy): an example of active block-resurgence in a densely populated area. J. Volcanol. Geotherm. Res. 91, 415–451. https://doi.org/10.1016/S0377-0273(99)00050-5.

Orsi, G., D'Antonio, M., Civetta, L., 2021. Campi Flegrei: A Restless Caldera in a Densely Populated Area.

Pandarinath, K., 2022. Application potential of chemical weathering indices in the identification of hydrothermally altered surface volcanic rocks from geothermal fields. Geosci. J. 26, 415–442. https://doi.org/10.1007/s12303-021-0042-2.

Peccerillo, A., Lustrino, M., 2005. Compositional variations of Plio-quaternary magmatism in the circum-Tyrrhenian area: deep versus shallow mantle processes. Special Paper of the Geological Society of America 388, 421–434. https://doi.org/10.1130/0-8137-2388-4.421.

Piochi, M., Kilburn, C.R.J., Di Vito, M.A., et al., 2014. The volcanic and geothermally active Campi Flegrei caldera: an integrated multidisciplinary image of its buried structure. Int. J. Earth Sci. 103, 401–421. https://doi.org/10.1007/s00531-013-0972-7.

Piochi, M., Mormone, A., Balassone, G., et al., 2015. Native sulfur, sulfates and sulfides from the active Campi Flegrei volcano (southern Italy): genetic environments and degassing dynamics revealed by mineralogy and isotope geochemistry. J. Volcanol. Geotherm. Res. 304, 180–193. https://doi.org/10.1016/j.jvolgeores.2015.08.017.

Piochi, M., Mormone, A., Balassone, G., 2019. Hydrothermal alteration environments and recent dynamics of the Ischia volcanic island (southern Italy): insights from repeated field, mineralogical and geochemical surveys before and after the 2017 Casamicciola earthquake. J. Volcanol. Geotherm. Res. 376, 104–124. https://doi.org/10.1016/j.jvolgeores.2019.03.018.

Rye, R.O., 2005. A review of the stable-isotope geochemistry of sulfate minerals in selected igneous environments and related hydrothermal systems. Chem. Geol. 215, 5–36. https://doi.org/10.1016/j.chemgeo.2004.06.034.

Savelli, C., Marani, M., Gamberi, F., 1999. Geochemistry of metalliferous, hydrothermal deposits in the Aeolian arc (Tyrrhenian Sea). J. Volcanol. Geotherm. Res. 88, 305–323. https://doi.org/10.1016/S0377-0273(99)00007-4.

Sbrana, A., Marianelli, P., Pasquini, G., 2018. Volcanology of Ischia (Italy). J. Maps 14, 494–503. https://doi.org/10.1080/17445647.2018.1498811.

Scarpati, C., Cole, P., Perrotta, A., 1993. The Neapolitan yellow tuff - a large volume multiphase eruption from Campi Flegrei, southern Italy. Bull. Volcanol. 55, 343–356. https://doi.org/10.1007/BF00301145.

Tassi, F., Capaccioni, B., Caramanna, G., et al., 2009. Low-pH waters discharging from submarine vents at Panarea Island (Aeolian Islands, southern Italy) after the 2002 gas blast: origin of hydrothermal fluids and implications for volcanic surveillance. Appl. Geochem. 24, 246–254. https://doi.org/10.1016/j.apgeochem.2008.11.015.

Tomlinson, E.L., Arienzo, I., Civetta, L., et al., 2012. Geochemistry of the Phlegraean fields (Italy) proximal sources for major Mediterranean tephras: implications for the dispersal of Plinian and co-ignimbritic components of explosive eruptions. Geochim. Cosmochim. Acta 93, 102–128. https://doi.org/10.1016/J.GCA.2012.05.043.

Yang, M., Liang, X., Ma, L., et al., 2019. Adsorption of REEs on kaolinite and halloysite: a link to the REE distribution on clays in the weathering crust of granite. Chem. Geol. 525, 210–217. https://doi.org/10.1016/j.chemgeo.2019.07.024.